의학박사 학위논문

Application of ZnO nanowires for intracellular delivery of biomacromolecules and cancer immunotherapy

산화아연 나노선을 활용한 생체고분자의 세포내 전달과 항암면역치료기술 연구

2019년 8월

서울대학교 대학원

의과학과 의과학 전공

Prashant Sharma

A thesis for the degree of Doctor of Philosophy

Application of ZnO nanowires for intracellular delivery of biomacromolecules and cancer immunotherapy

산화아연 나노선을 활용한 생체고분자의 세포내 전달과 항암면역치료기술 연구

August 2019

Major in Biomedical Sciences

Department of Biomedical Sciences

Seoul National University

Prashant Sharma

Application of ZnO nanowires for intracellular delivery of biomacromolecules and cancer immunotherapy

By

Prashant Sharma

A thesis submitted to the Department of Biomedical Sciences for the fulfillment of the requirement of the degree of Doctor of Philosophy in Medical Sciences at

Seoul National University

August 2019

Approved by Thesis committee:

Professor Seung-Yong Seong **Chairman**

Professor Hoonchul Kwon **Vice-chairman**

Professor Dae-Ho Lee

Professor

Professor Young Keun Kim

1. Abstract

Zinc oxide (ZnO) nanocomposites have been widely applied in biomedical fields due to their multifunctionality and biocompatibility. However, the physicochemical properties of ZnO nanocomposite involved in nano–bio interactions are poorly defined. To assess the potential applicability of ZnO nanowires for intracellular delivery of biomolecules, I examined the dynamics of cellular activity of cells growing on densely packed ZnO nanowire arrays with two different physical conformations, vertical (VNW) or fan-shaped (FNW) nanowires. Although a fraction of human embryonic kidney cells cultured on VNW or FNW underwent rapid apoptosis, peaking at 6 h after incubation, cells could survive and replicate without significant apoptosis on the foreign substrate after 12 h of lag phase. In addition, the cells formed lamellipodia to wrap FNW, and efficiently took up peptides non-covalently coated on VNW and FNW within 30 min of incubation. Moreover, FNW could mediate intracellular delivery of associated DNAs and their gene expression, suggesting that ZnO nanowires transiently penetrate membranes to mediate intra-nuclear delivery of exogenous DNA. These results indicate that ZnO nanowire arrays can serve as nanocomposites for manipulating nano–biointerfaces if appropriately modified in a 3-dimensional conformation. Radially grown ZnO nanowires on poly-L-lactic acid (PLLA) microfibers with the unique 3-dimensional structure were also synthesized and applied as therapeutic cancer vaccines. This inorganic-organic hybrid nanocomposite has mild cellular toxicity but efficiently delivers a tumor antigen into dendritic cells, cellular bridges between innate and adaptive

immunity, to stimulate them to express inflammatory cytokines and activation surface markers. I also demonstrated that the hybrid nanocomposites successfully induce tumor antigen-specific cellular immunity and significantly inhibit tumor growth *in vivo*. ZnO nanowires on PLLA fibers systemically reduced immune suppressive T_{reg} cells and enhanced the infiltration of T cells into tumor tissues, compared to mice immunized with PLLA fibers coated with the antigen. These findings open a new avenue in extending the biomedical application of inorganic metal oxide-inert organic hybrid nanocomposites as a novel vaccine platform.

*This work is published in following journals.

Sharma, P., Shin, J.B., Park, B.C., Lee, J.W., Byun, S.W., Jang, N.Y., Kim, Y.J., Kim, Y., Kim, Y.K. and Cho, N.H., Application of radially grown ZnO nanowires on poly-l-lactide microfibers complexed with a tumor antigen for cancer immunotherapy. Nanoscale (2019), 11 (10), 4591-4600.

Sharma, P.; Cho, H. A.; Lee, J. W.; Ham, W. S.; Park, B. C.; Cho, N. H.; Kim, Y. K., Efficient intracellular delivery of bio-macromolecules employing clusters of zinc oxide nanowires. Nanoscale (2017), 9 (40), 15371-15378.

Keywords: Zinc oxide nanowire, intracellular delivery, poly-L-lactic acid microfiber, zinc oxide-binding peptide, inorganic-organic hybrid, cancer immunotherapy

Student number: 2013-30817

2. Contents

3. List of Figures

Chapter 1.

Chapter 2.

4. List of Abbreviations

APCs: Antigen-presenting phagocytic cells

AP: Alkaline phosphatase

BSA: Bovine serum albumin

CTL: Cytotoxic T lymphocyte

CEA: Carcinoembryonic antigen

DMSO: Dimethyl sulfoxide

DC: Dendritic cell

EMSA: Electrophoretic mobility shift assay

EDTA: Ethylenediaminetetraacetic acid

FITC: Fluorescein isothiocyanate

FE-SEM: Field emission scanning electron microscope

FNW: Fan-shaped nanowires

GFP: Green fluorescent protein

HEK: Human embryonic kidney

IL-1β: Interleukin 1 beta

IL-6: Interleukin 6

IL-10: Interleukin 10

IFN-γ: Interferon gamma

IPTG: Isopropyl β-D-1-thiogalactopyranoside

LPS: Lipopolysaccharide

MHC: Major histocompatibility complex

MARCO: Macrophages expressing the scavenger receptor

NWs: Nanowires

PLLA: poly-L-lactic acid

PLGA: poly lactic-co-glycolic acid

PBS: Phosphate buffer saline

PCR: Polymerase chain reaction

ROS: Reactive oxygen species

7-AAD: 7-aminoactinomycin D

TEM: Transmission electron microscope

T_{reg}: Regulatory T cells

TLR: Toll-like receptor

TNF-α: Tumor Necrosis Factor-α

3D: Three-dimensional

VNW: Vertical nanowires

XRD: X-ray diffraction

ZnO: Zinc oxide

ZBP: ZnO-binding peptide

5. General Introduction

Zinc oxide (ZnO) has long been used in our daily life as ingredients of medicine, cosmetics, and food additives. Piezoelectric ZnO has also been widely applied in optoelectronics, sensors, transducers, energy conversion [1-3]. ZnO is a metal oxide semiconductor material with a direct wide band gap energy (3.37 eV) and a large exciton binding energy (60 meV) at room temperature [1]. ZnO crystallize in either cubic zinc-blende or hexagonal wurtzite structure where each anion is surrounded by four cations at the corners of a tetrahedron, and vice versa. The crystal structures shared by ZnO are wurtzite, zinc blende, and rocksalt. The hexagonal wurtzite is the most stable phase thermodynamically [1]. Medical application of ZnO has a long history. For example, a probable form of ZnO, named as Pushpanjan, for eyes and open wound treatment is mentioned in the Indian ancient medical textbook, the Charaka Samhita which was written around 500 B.C. [4]. ZnO lotion is introduced by a Greek physician, Dioscorides, in the first century A.D. Avicenna, a Persian philosopher, and physician, also discussed about ZnO in his book, The Canon of Medicine, as a preferred cure for a multiple skin diseases, including skin cancer [4]. ZnO has been produced by heating zinc ore in a shaft furnace. The liberated metallic zinc as a vapor, which then ascended the flue and condensed as the oxide for various applications [5-6].

Historic and modern evidences suggest potential applicability of ZnO in biomedical sciences. Biodegradability and low toxicity of ZnO nanomaterials also underscore the relevance of their biomedical applications [2]. ZnO nanocrystals and nanostructures have been employed for the

luminescence imaging of cells [7]. RGD peptide-conjugated ZnO exhibiting green luminescence demonstrated that the nanowires are useful for molecularly targeted imaging of cancer cells [8]. Other studies have shown that biomolecule penetration inside the cells can be a useful tool for in-depth cytology, modeling, and simulation of gene circuits, as well as antigen delivery for immunotherapy [10-11]. However, ZnO nanowires (NWs) have been poorly characterized for biomedical application, and there have been only a few reports for the use of the biological field [11]. Even though it has been shown that zinc has a positive effect on the immune system, [12-14] only a few reports have shown the uses of ZnO nanocomposites as immune modulator. In a recent study, ZnO nanoparticle was shown to have adjuvant potential when combined with vaccine antigen [15]. ZnO also enhances the innate immune responses via stimulation of TLR6-mediated signaling [15-17]. In another report, ZnO nanoparticles have shown to promote antigen uptake by dendritic cells [18]. Additionally, ZnO nanoparticles or mesoporous ZnO has also shown to have a potent anti-cancer effect [19-21].

In this study, I have extensively analyzed nano-bio interfaces by using ZnO nanowires in various three-dimensional forms and investigated the possible correlation of the physical conformation of the 3D structures with cytotoxicity and efficacy of intracellular delivery of associated bio-macromolecules. In addition, I investigated the potential application of ZnO nanowires, forming a unique 3D structure on poly-L-lactic acid (PLLA) microfibers, a biocompatible organic matrix, as an immunotherapeutic adjuvant system for cancer immunotherapy. Radially grown ZnO nanowires on PLLA fibers were complexed with a tumor antigen, carcinoembryonic

antigen (CEA), to be exploited as a novel intracellular antigen delivery system. The immune stimulatory effect of the inorganic-organic hybrid nanocomposites was confirmed *in vitro* using phagocytic dendritic cells. Immunization with the CEA-coated hybrid nanocomposites not only enhanced antigen-specific T cell responses, but also suppressed tumor growth significantly better than PLLA fibers mixed with CEA in an *in vivo* mouse model, demonstrating that incorporation of ZnO nanowires into the inorganic-organic hybrid composite has promising potential as a vaccine adjuvant for antigen delivery as well as immune stimulation.

6. Chapter 1

Efficient intracellular delivery of biomacromolecules employing clusters of Zinc oxide nanowires

6.1. Introduction

Zinc oxide (ZnO) is a unique material that exhibits exceptional semiconducting, piezoelectric, and pyroelectric properties so have therefore been widely applied in nano-electronics, optoelectronics, sensors, light-emitting diodes, photo-catalysis, nano-generators, and nanopiezotronics [1-2]. The metal oxide has also been applied in food, UV-blocking agents, and anti-microbial materials, due to its multi-functionality and biocompatibility.

ZnO-based nanocomposites have shown promising potential in bio-imaging, drug delivery, and immunotherapy during the last decade [15, 57, 18]. Previously, ZnO nanoparticles chemically conjugated with acid-sensitive polymers were shown to be taken up by cancer cells through endocytosis, and release a preloaded anti-cancer drug into cellular lysosomes in a pH-dependent manner [34]. It was also reported that an iron oxide–ZnO core-shell nanoparticle can efficiently deliver a tumor antigen fused with ZnO-binding peptide (ZBP) into dendritic cells and potently enhance antigen-specific immunity *in vivo* when applied for cancer immunotherapy [18]. It appears that ZnO nanoparticle itself possesses adjuvant potential as a vaccine carrier when combined with an antigen having high affinity to the metal oxide [15].

In addition to chemical drugs and protein antigens, plasmid DNA can also be delivered and expressed in eukaryotic cells when associated with ZnO nanostructures [11, 35]. Silica-coated and amino-modified tetrapod-like ZnO nanostructures can bind plasmid DNA through electrostatic interactions and mediate intracellular delivery and expression of the associated DNA in mammalian cells [11]. The unique three dimensional (3D) structure of ZnO

tetrapods might be important for the direct delivery of DNA and its gene expression in eukaryotic cells since there was no detectable gene expression when using silica and DNA coated simple ZnO nanorods [11]. Recently, it was also reported that ZnO nanowires conjugated to DNA via disulfide bonds could also deliver nucleic acids into rigid algal cells after physical pressurization, and result in better gene expression compared to traditional bead beating and electroporation [35]. These results indicate that ZnO nanostructures can be applied as delivery vehicles for bio-macromolecules, such as proteins and DNA, into eukaryotic cells with appropriately modified surfaces and 3D structures, or with physical force. However, detailed mechanisms of how ZnO nanostructures mediate intracellular delivery of associated bio-macromolecules remain elusive.

In addition, ZnO nanocomposites are known to exert cytotoxicity depending on their size, shape, surface modification, and concentration [21-24, 36-37]. The effect of 3D structure on biological systems has been poorly defined, and most studies use spherical ZnO nanoparticles, which are readily internalized into cells by endocytosis or phagocytosis [18, 36]. The cytotoxic potential of ZnO nanoparticles is generally attributed to dissolution of the metal oxide complex into Zn^{2+} ions, especially in acidic environments such as lysosomes [38]. Cellular uptake of ZnO nanoparticles may facilitate an increase in intracellular Zn^{2+}, leading to rapid perturbation of cellular Zn^{2+} homeostasis, which ultimately induces reactive oxygen species (ROS) generation, DNA damage, and apoptotic cell death [36]. Previously, it was shown that the toxic potency of ZnO tetrapods in the nano-micron size range is significantly lower than that of spherical ZnO nanoparticles, [39, 40]

indicating that physical constraints of 3D structure may limit the intracellular uptake of the complex so that less Zn^{2+} ions are generated, thereby reducing cellular toxicity. Nevertheless, direct contact of ZnO nanowires in the tetrapods with cells, induced a degree of cellular toxicity, potentially due to local generation of Zn^{2+} or physical damage [39-41]. Therefore, the primary factors of ZnO nanocomposite that induce biological toxicity as well as influence the efficacy of intracellular delivery of associated bio-macromolecules need to be further defined to improve their biological applicability.

In this study, densely packed ZnO nanowire arrays with two different physical arrangements, vertical and fan-shaped forms, synthesized by a hydrothermal method [41] were used for biological application, especially for intracellular delivery of bio-macromolecules. I investigated the possible correlation of the physical conformation of the 3D structures with cytotoxicity and efficacy of intracellular delivery of associated bio-macromolecules.

6.2. Material Methods

6.2.1. Synthesis of ZnO nanowire

ZnO nanomaterials were synthesized as follows and supplied by Professor Young Keun Kim's laboratory, Korea University. The ZnO nanoparticles, which act as seeds were synthesized using 50 mM $Zn(NO_3)•6H_2O$, 12 mM cetyltrimethylammonium bromide (CTAB) in ethanol and an equivalent volume of 0.1 M NaOH in ethanol. This solution was washed with ethyl alcohol using an ultrasonic cleaner and centrifuged after vigorous stirring for one hour to precipitate the ZnO nanoparticles [42]. Two types of ZnO nanowire arrays were synthesized by a hydrothermal method. A ZnO thin layer and ZnO nanoparticles were used as seed layers. The cover glasses were cleaned by sonication in acetone, ethyl alcohol, and deionized water. ZnO layer (100 nm), Seed layers were deposited on the substrates by a dc magnetron sputtering system. ZnO nanoparticles which were suspended in the diluted solution (10 μg/ml) were dropped over the substrates. A 10 mM of zinc nitrate hexahydrate ($Zn(NO_3)•6H_2O$), and 10 mM of hexamethylenetetramine (HMTA, $C_6H_{12}N_4$) were dissolved in deionized water to synthesize the ZnO nanowire arrays on the seeded cover glass. Additionally, 2 mM of polyethyleneimine (PEI, branched, low molecular weight, Aldrich) and 6 mM of ammonium chloride (NH_4Cl) were supplemented to increase the length and to decrease the diameter of ZnO nanowires [43-45]. The prepared solution was heated in the oil bath to maintain uniform temperature during the synthesis of the ZnO nanowires. The

seeded cover glasses were dipped into the solution at a growth temperature of 95ºC for 2 h. After the reaction, the cover glasses were removed from the solution, and rinsed with deionized water.

6.2.2. Cell viability assay

Cell viability was determined by Trypan blue and Apoptosis assay. HEK293T cells grown on nanowires were observed at different time intervals during a period of 1 h to 96 h. After incubation, the cells were trypsinized with 0.05% trypsin solution. Ten microliter cell suspension mixed with 10 µl Trypan Blue. The 10 µl mixture was added into the hemocytometer, and the live cell amount under an optical microscope was counted to calculate the total number of cells. Annexin V-Alexa Fluor 568 (eBioscience, USA) and 7-AAD double staining used for apoptosis of HEK293t cells on Nanowires was assayed by flow cytometer (BD Biosciences, USA). After treatment with FNW and VNW for 1 h to 96 h, cells were harvested with trypsin, washed twice with cold PBS, and resuspended in 200 µl binding buffer. Cells were transferred to a 1.5 ml culture tube, added to by 5 µl of Annexin V-Alexa Fluor 568, incubated at 4°C in the dark for 15 min, and then added 5 µl of 7-AAD in the dark.

6.2.3. Electron microscopy

The morphology and structure of the nanowire arrays are investigated by using a field emission scanning electron microscope (FE-SEM, S-4300, Hitachi, Japan), transmission electron microscope (TEM, JEM-2100F, JEOL) as well as high-resolution transmission electron microscopy (HRTEM), and

X-ray diffraction (XRD, D/MAX-2500 V/PC, Rigaku, Japan). Cells grown on the nanowire-coated coverslips were also examined by SEM. After washing with phosphate-buffered saline (PBS), the cells were fixed with glutaraldehyde and sodium cacodylate solution (Karnovsky Fixate) for 2 h. Samples were rinsed with a 1% solution of osmium tetroxide in 0.1 M sodium cacodylate for 2 h, serially dehydrated with increasing concentrations of ethanol, critical point dried with hexamethyldisilazane, and then sputter-coated with a platinum/palladium film. The samples were examined using a scanning electron microscope (Hitachi S4700, Japan) at an accelerating voltage of 15 kV.

6.2.4. Binding of ZnO-binding peptides on nanowires

Indicated amounts of ZnO-binding peptides (ZBP, amino acid sequences: RPHRKGGDARPHRKGGDARPHRKGGDA) labeled at their carboxyl terminals with fluorescein isothiocyanate (FITC, Peptron, Korea) were incubated with ZnO nanowires on a coverslip for 1 h at 37°C. The ZnO nanowires coated with ZBP-FITC were washed 3 times using PBS and then the relative binding of ZBP-FITC was assessed by measuring the fluorescence intensity using Infinite®M200 PRO (Taken, Switzerland) or used for cell culture.

6.2.5. Confocal microscopy and flow cytometry

ZnO nanowire-coated coverslips were incubated with 100 μM of ZBP-FTIC at 37°C for 1 h and washed 3 times using PBS to remove unbound peptides. Subsequently, HEK293 cells were seeded and incubated at 37°C for the

indicated time. The cells were fixed in 4% paraformaldehyde at room temperature for 20 min and permeabilized using 0.2% Triton X100 (Sigma-Aldrich, USA) in PBS for 15 min. Cellular nuclei and actin cytoskeletons were stained with TO-PRO-3 (Molecular Probes, USA) and Alexa Fluor594-Phalloidin conjugate (Molecular Probes, USA), respectively, according to the manufacturer's instruction. The stained cells were washed 3 times with PBS and observed using an Olympus FV1000 laser confocal microscope (Olympus, Japan) and analyzed using the Fluoview software (Olympus, Japan). The cellular uptake of ZBP-FITC or GFP expression was examined after harvesting the cells from the coverslips using a flow cytometer (LSR II, BD Biosciences, USA).

6.2.6. Intracellular delivery of peptides by endocytosis or penetration

Cell Culture Media, centrifuge, nanwire coverslips maintained at Room temperature, 4°C and 37°C. After trypsinization, HEK 293T cells had been plated on the coverslips and centrifuged, HEK 293T cells with ZBPFITC nanowires and incubated at 4°C and 37°C for 5 min or 30 min and collected for FACS analysis to analyze temperature effect on intracellular delivery of peptides.

6.2.7. Preparation of ZBP–streptavidin and biotin–DNA complex

A reporter DNA encoding GFP expression cassette was amplified using a

PCR primer set (forward primer: 5′-biotinylated atagtaatcaattacggggtcattag-3′, reverse primer: 5′-tgaaaaaaatgctttatttgtgaaatt-3) and pEGFP-N1 vector (Clontech, USA) as a template. To generate ZnO NW and the biotinylated DNA complex, I produced recombinant ZBP–streptavidin protein. First, DNA encoding streptavidin was amplified by using a primer set (forward primer: 5′-gaattcagctgaagctggtatcacc-3′, reverse primer: 5′-ctcgaggtgatgggaagcagcgga-3′, EcoRI, and XhoI sites underlined) and pET21a-Streptavidin-Alive plasmid [27] (Addgene, USA) as a template. The DNA encoding streptavidin was ligated into pET28a vector containing the ZBP-encoding sequences (5′-cgcccgcatcgcaaaggcggcgatgcgcgcccgcatcgcaaaggcggcgatgcgcgcccgcatcgcaaa ggcggcgatgcg-3) after the DNA restriction. The recombinant plasmid encoding ZBP–streptavidin protein (pET28a/ZBP–streptavidin) was introduced into *E. coli* BL21 (DE3) strain (RBC biosciences, Taiwan). ZBP–streptavidin protein was induced in the recombinant E. coli by using 0.1 mM isopropyl β-D-thiogalactoside (IPTG; Duchefa Biochemie, Netherlands) at 16°C for 16 h and purified using Ni-NTA resin (Thermo Fisher Scientific, USA) according to the manufacturer's instruction.

6.2.8. Electrophoretic mobility shift assay (EMSA)

The electrophoretic mobility shift assay was performed to confirm the complex formation of ZBP–streptavidin and biotinylated DNA, as previously described [46]. Briefly, 20 μg of biotinylated DNA was incubated with an indicated amount of ZBP–streptavidin at room temperature for 1 h. The resulting ZBP–streptavidin/biotin–DNA complexes were loaded on 1% agarose gel and visualized under UV light after electrophoresis in the

presence of ethidium bromide.

6.2.9. Functionalizing nanowires and DNA transfection

Coverslips were transferred into a 24 well cell culture plate, washed with 70% ethanol, and sterilized under UV for 1 h. Purified ZBP–streptavidin protein (80 μg) complexed with biotinylated DNA encoding GFP (20 μg) were added to the well containing a coverslip and incubated at 37°C for 1 h. The unbound complexes were removed by washing with PBS, and HEK293 cells (5×10^4 cells per well) were plated. GFP expression in the cells was analyzed using confocal microscopy and flow cytometry as described above.

6.2.10. Statistical analysis

Data were analyzed using the Graph Pad Prism 5.01 software (Graph Pad Software, USA). Statistical analysis was performed using One-way ANOVA. Data are expressed as the mean ± standard deviation. The p-value less than 0.05 was considered statistically significant.

6.3. Results

6.3.1. Characterization of ZnO nanowire

Morphological features of vertical (VNW) and fan-shaped (FNW) nanowires arrayed on glass coverslips prepared with a ZnO seed layer and ZnO nanoparticles, respectively, are presented in Fig. 1-1 A–D. The diameters of the ZnO nanowires range from 100 to 200 nm with lengths of 0.5 to 2.5 μm. X-ray diffraction (XRD) patterns of VNW and FNW confirm the characteristic peaks of ZnO with a hexagonal wurtzite structure (Fig. 1-2). Microstructural features of VNW and FNW are represented in Fig. 1-1 E–G. The selected area electron diffraction (SAED) pattern of the individual ZnO nanowire showed clear spots, confirming that the nanowire has a single-crystalline wurtzite structure (Fig. 1-1 F). The spots can be indexed by (1010) and (0002) planes, where the d spacing is 0.161 nm for the (1010) plane (d (1010)) and 0.257 nm for the (0002) plane (d (0002)). Furthermore, the SAED pattern indicates that the ZnO nanowire was synthesized along the [0002] direction. The lattice fringes in the high-resolution transmission electron microscopy (HRTEM) image of Fig. 1-1 G are distinct, and the d spacing of the (0002) plane (d(0002)) measured from the fringe spacing of HRTEM is 0.252 nm. These results match well with the d (0002) of 0.260 nm and 0.257 nm derived from XRD and SAED, respectively.

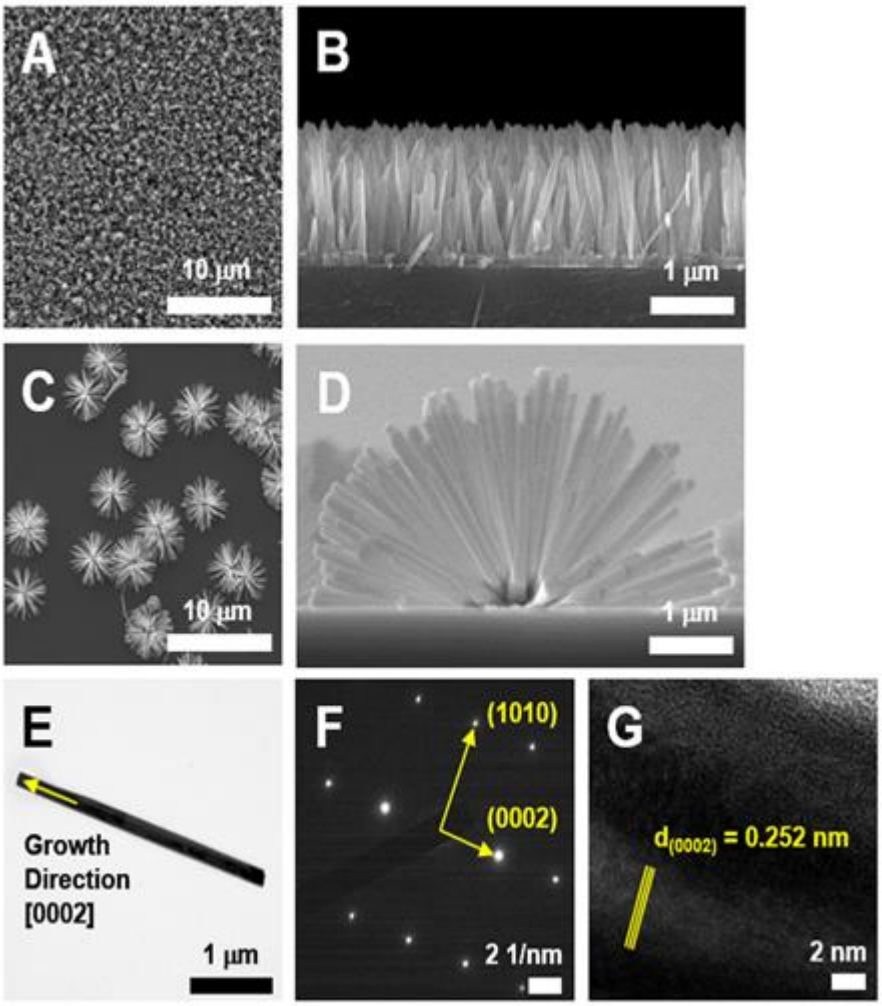

Figure 1-1. Morphological and microstructural analysis of ZnO nanowire arrays. Scanning electron microscopy (SEM) images present densely packed vertical ZnO nanowires (A. top view, B. side view) and fan-shaped nanowires (C. top view, D. side view). (E) Bright-field transmission electron microscopy (TEM) image is showing a single ZnO nanowire. The yellow arrows indicate the growth direction of [0002]. (F) Selected area electron diffraction (SAED)

spot pattern of the ZnO nanowire. (1010) and (0002) planes are indexed. (G) High-resolution TEM image of the ZnO nanowire. The solid yellow lines indicate a lattice fringe of the (0002) plane with a d spacing of 0.252 nm.

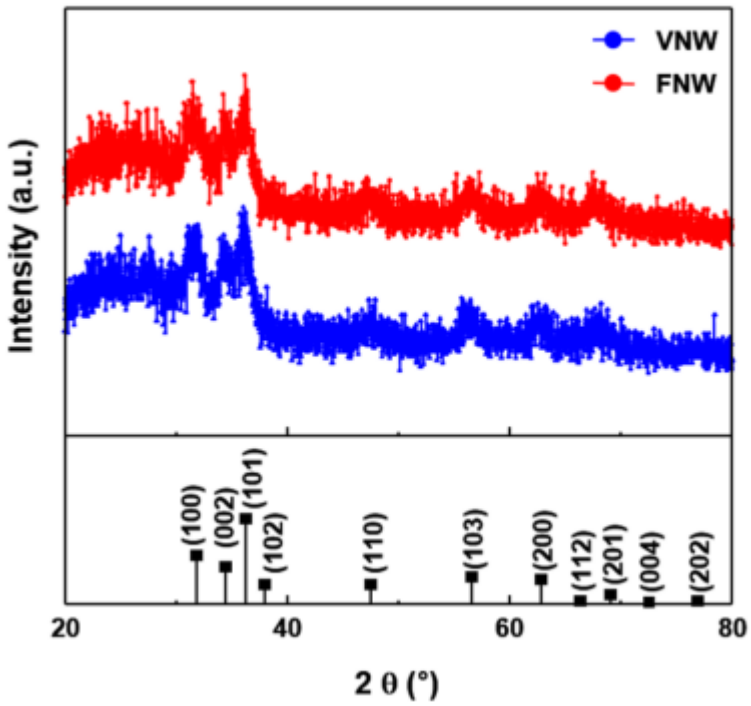

Figure 1-2. XRD patterns of vertical ZnO nanowire (VNW) and fan-shaped ZnO nanowire (FNW) arrays. The characteristic peaks of wurtzite ZnO (JCPDS No. 36-1451) are denoted in the bottom part of the graph.

6.3.2. Cellular toxicity of ZnO nanowires

In order to assess the cellular toxicity of ZnO nanowires, HEK293 cells were grown on VNW or FNW, and live cell counts were compared with those grown on a normal glass coverslip (Fig. 1-3). Live cell counts gradually increased in all the cultures after 12 h of lag phase, indicating that the HEK293 cells can replicate on glass coverslips coated with VNW or FNW arrays, albeit with a slightly lower growth rate than that of the normal coverslip (Fig. 1-3 A). To assess potential toxicity during the lag phase, I examined cellular necrosis and apoptosis (Fig. 1-3 B-C). Apoptotic cell death was detected as early as 1 h after incubation with VNW or FNW arrays, suggesting that apoptosis is rapidly induced upon direct contact with ZnO nanowires. It gradually increased up to 6 h after incubation and then decreased thereafter. Even though induction of apoptosis was also observed in the cells inoculated onto normal glass coverslips, ZnO nanowire itself, regardless of VNW or FNW, significantly enhanced apoptotic cell death more than a normal glass surface. The cells on FNW showed relatively higher rates (~40%) of apoptosis during the early stage (~3 h) of exposure when compared to those of the cells on VNW (~26%) or normal coverslips (~30%). Late apoptotic cells positive for both 7-aminoactinomycin D (7-AAD) and Annexin V peaked at 6 h after incubation in all the experiment sets. The cells incubated on VNW and FNW showed significantly higher rates (33–35%) of late apoptotic phenotype than the cells on glass coverslips without nanowires (~14%). Interestingly, necrotic cells were barely detected up to 3 h after incubation, but transiently peaked at 3–6% of cells in all the experimental sets at 6 h after inoculation, indicating that direct necrotic

damage, as measured by membrane penetration of 7-AAD without annexin V staining, follows cellular apoptosis.

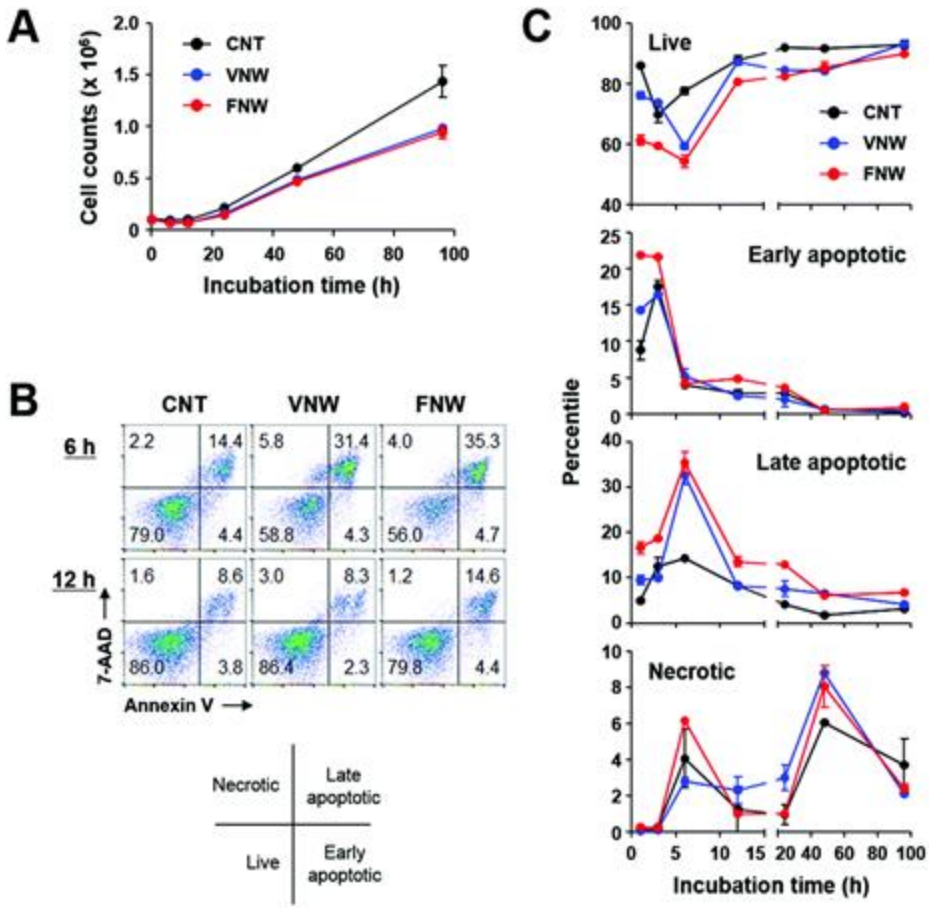

Figure 1-3. The effect of ZnO nanowire arrays on cell viability. (A) HEK293 cells were grown on glass coverslips (CNT), including vertical nanowires (VNW) or fan-shaped nanowires (FNW), and their growth was monitored for up to 96 h. (B and C) Cellular apoptosis and necrosis were assessed by flow cytometry after annexin V and 7-AAD staining at the indicated times after cell culture.

6.3.3. Zinc oxide-binding peptide binding assay

The zinc oxide-binding peptide was identified and analyzed in a previous study [18]. I analyzed the binding of ZnO nanowires, and FITC tagged Zinc binding peptide. A concentration of 10 to 320μM of ZBPFITC was incubated with FNW and VNW nanowires. At 80 μM, both the nanowires showed saturation (Fig.1-4).

6.3.4. Cellular responses during the culture on ZnO nanowires

I further examined the cells grown on VNW or FNW when they were actively dividing by imaging analysis (Fig. 1-5). Scanning electron microscopy showed that the surface morphology of the cells on nanowire-coated coverslips was similar to those of the cells grown on the normal cover glass after 24 h of incubation (Fig. 1-5 A). At 48 h of incubation, the cells on nanowire-coated coverslips can replicate as efficiently as those on normal glass slips and gradually cover the whole surface area (Fig. 1-5 B). When cellular actin and nuclei were stained, however, the cells grown on FNW showed a distinct arrangement and morphology of actin cytoskeletons and nuclei compared to those of the cells grown on normal coverslips and VNW (Fig. 1-5 B and C). Deformed nuclei were often observed in the cells that cover multiple FNW clusters. Actin cytoskeletons surround clusters of FNW and form lamellipodia at contact edges (Fig. 1-5 C).

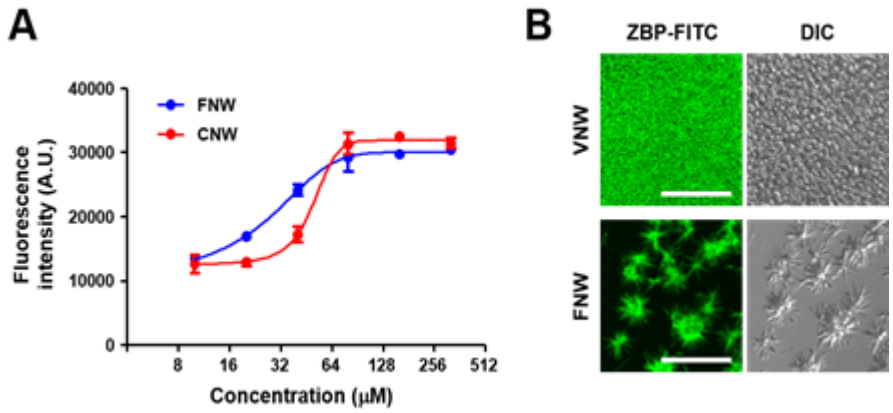

Figure 1-4. Coating of ZnO nanowire arrays with ZBP-FITC. (A) Vertical (VNW) or fan-shaped (FNW) nanowires were incubated with indicated concentration of ZnO-binding peptides (ZBP) conjugate with FITC for 1 h at 37˚C. ZnO nanowire arrays coated with ZBP-FITC were assessed the relative binding of ZBP-FITC by measuring the fluorescence intensity. (B) Representative images of ZnO nanowire arrays coated with ZBP-FITC. DIC, differential interference contrast. White bar, 10 μm.

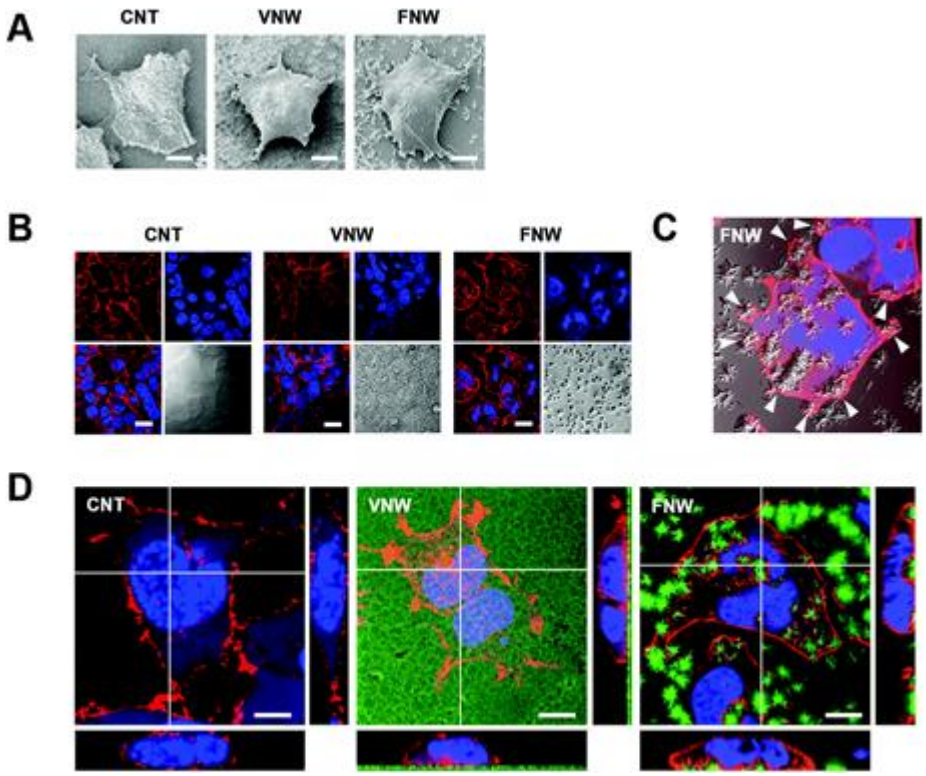

Figure 1-5. Morphology of cells grown on ZnO nanowire arrays. (A) SEM images of HEK293 cells grown on glass coverslips (CNT), vertical nanowires (VNW), and fan-shaped nanowires (FNW) at 24 h after cell culture. (B and C) Cells grown on nanowire arrays for 48 h were stained with TO-PRO-3 and Alexa Fluor594-Phalloidin conjugate to observe cellular nuclei (blue) and the actin cytoskeleton (red), respectively. Magnified image of cells grown on FNW shows deformed nuclei and distinct arrangement of actin cytoskeletons, lamellipodia, surrounding the ZnO nanowire clusters at the contact edges (C, white arrowheads). (D) Cells were grown on nanowire arrays coated with ZBP-FITC (green) for 24 h, and cell nuclei and actin cytoskeleton were

stained with TO-PRO-3 and phalloidin. Fluorescence images of cells and ZnO nanowires were assessed by confocal scanning of z-stacks and orthogonal views (yz and xz) are shown in the right and bottom panels. Excitation (ex.) and emission (em.) wavelengths for detecting the fluorescent probes by confocal microscopy are as follows; FITC: ex. 495 nm, em. 519 nm, Alexa Fluor594-Phalloidin: ex. 581 nm, em. 609 nm, and TO-PRO-3: ex. 642 nm, em. 661 nm. White bar, 10 μm.

6.3.5. Intracellular uptake of peptides coated on ZnO nanowires

In order to observe the structures at the contact area between the cells and nanowires in more detail, I applied ZnO-binding peptide (ZBP) conjugated with FITC. The binding of ZBP-FITC to VNW or FNW was measured at titrated concentrations of ZBP-FITC after incubation for 1 h and binding of ZBP-FITC was measured by fluorescence intensities and fluorescent microscopy (Fig. 1-4). Then, cells were cultured on VNW or FNW coated with ZBP-FITC for 24 h and observed under a confocal microscope. A 3D reconstitution of confocal scanning images shows actin cytoskeleton and lamellipodia formation at the contact edges with FNW, whereas gross organization of the cellular structures grown on VNW was similar to those of the cells grown on normal coverslips (Fig. 1-5 D). It is also notable that the deformation of nuclei of the cells grown on FNW is primarily caused by spatial constraint of nanowire clusters.

To investigate the cellular mechanisms involved in the delivery of peptides, peptide-coated nanowire arrays were incubated with cells at 4°C for 30 min, and the cell uptake of FITC-labelled peptides was measured by flow cytometry. As seen in Fig. 1-6 C, intracellular delivery of peptide was remarkably reduced when cells were incubated at 4°C with VNW and FNW, suggesting that active cellular processes such as endocytosis may play a significant role in the intracellular uptake of peptides on the nanowires. Nevertheless, a proportion of cells were still positive for the FITC signal, suggesting that a direct penetration of the peptides into the cells may also occur. More efficient intracellular delivery was consistently observed when

cells were incubated at 4°C with FNW (60%) than with VNW (25%) (Fig. 1-6 C and D).

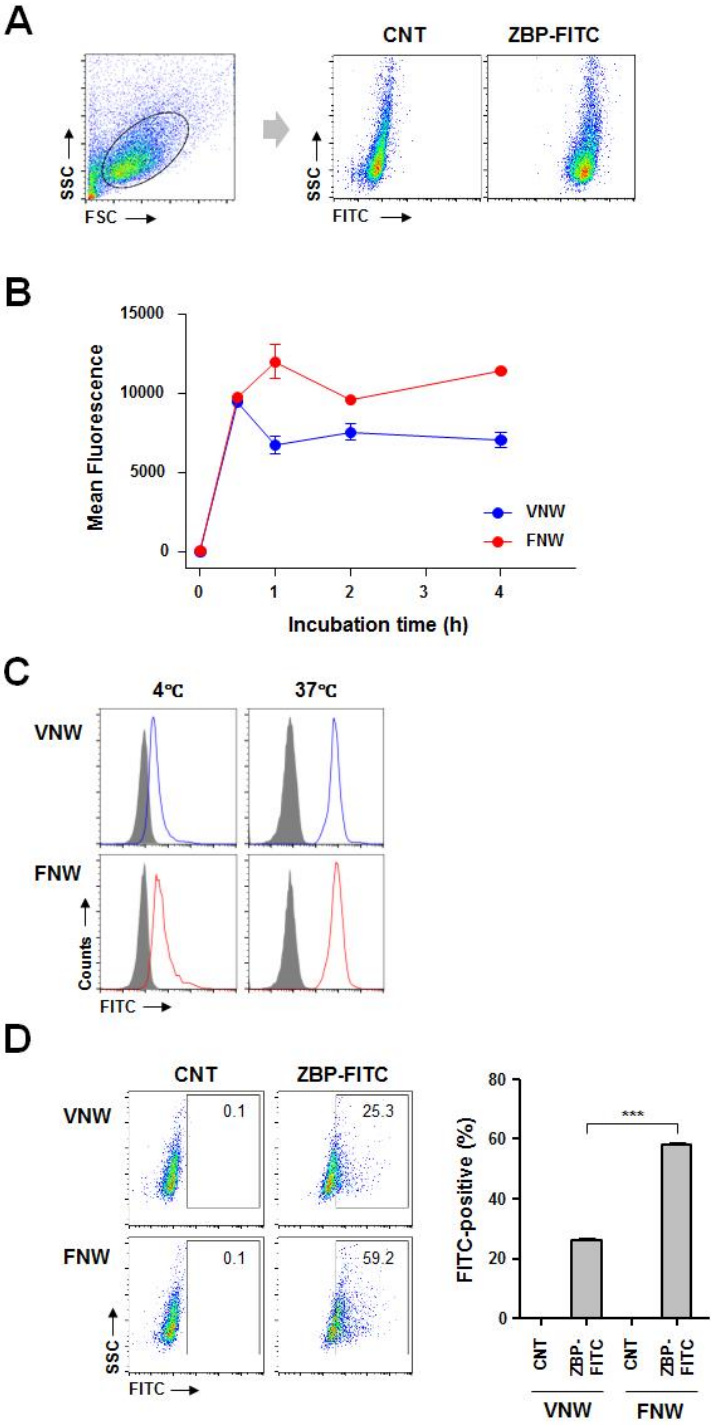
A
CNT
ZBP-FITC
SSC
FSC
SSC
FITC
B
15000
10000
5000
0
Mean Fluorescence
VNW
FNW
0
1
2
3
4
Incubation time (h)
C
4℃
37℃
VNW
FNW
Counts
FITC
D
CNT
ZBP-FITC
VNW
0.1
25.3
FNW
0.1
59.2
SSC
FITC
80
60
40
20
0
FITC-positive (%)
***
CNT
ZBP-FITC
CNT
ZBP-FITC
VNW
FNW

Figure 1-6. Intracellular uptake of peptides coated on ZnO nanowires.

(A and B) HEK293 cells were incubated on ZnO nanowire arrays coated with ZBP-FITC at 37°C for the indicated times and analyzed by flow cytometry. Live cells were gated based on a scatter plot. Mean fluorescence intensities of cells from triplicated assays are presented (B). (C) Flow cytometric analysis of cells incubated on ZnO nanowire arrays coated with ZBP-FITC either at 4°C or 37°C for 30 min. Cells incubated on nanowire arrays without ZBP-FITC coating were presented as gray histogram and cells on those coated with ZBP-FITC are presented as blue (VNW) or red (FNW) histograms. (D) Cells were incubated at 4°C on VNW and FNW coated with ZBP-FITC for 30 min and collected for FACS analysis. Representative flow cytometric scatter plots (left panels) and the graph showing the percentage of FITC positive cells from triplicated experiments (right panel) are presented. CNT: nanowires without ZBP-FITC coating, VNW: vertical nanowires, FNW: fan-shaped nanowires. Error bars indicate SD of experimental replicates ($n = 3$) ***, $p < 0.001$.

6.3.6. Saturation of ZBP streptavidin binding on nanowires

To confirm the binding saturation of a protein on nanowires, 300 µg of ZBP streptavidin incubated for a different time interval. The unbound protein is collected and checked for the concentration using BSA assay. It was confirmed that 150 µg of ZBP streptavidin protein get saturated on ZnO nanowires, after the 4 h of incubation at 37^{o}C (Fig. 1-7 A-B).

6.3.7. Analysis of ZBP streptavidin protein-biotinylated DNA binding

Electromobility shift assay (EMSA) confirms ZBP streptavidin and biotinylated GFP DNA binding on ZnO nanowires. When biotinylated DNA (20 µg) was incubated with 10, 20, 40, 80, or 160 µg of ZBP streptavidin for 1 h, approximately 80 µg ZBP streptavidin protein is sufficient to bind ~ 90 % of input DNA as visualized by gel electrophoresis and quantification by ImageJ software (Fig. 1-7 C-D).

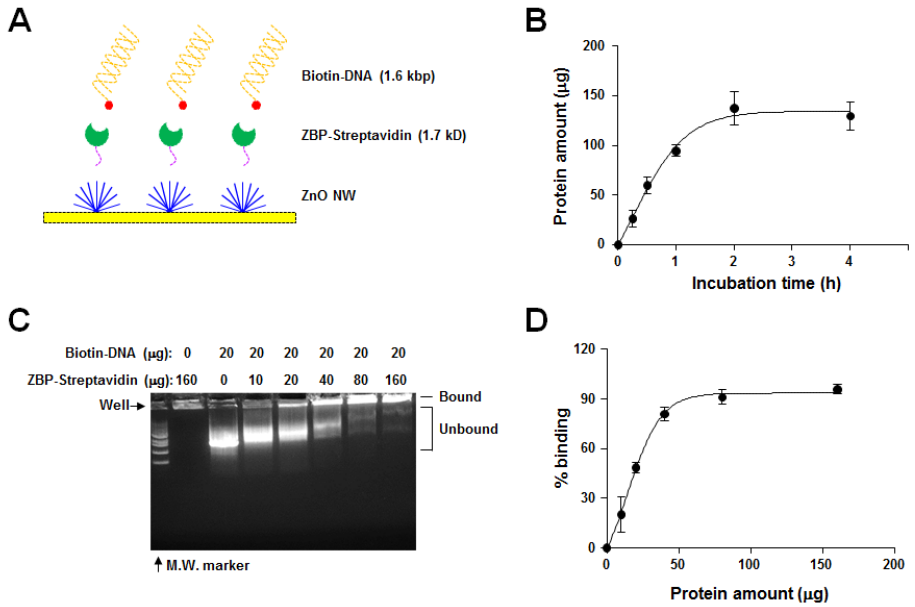

Figure 1-7. Complex formation of ZBP-streptavidin and biotin-labeled DNA. (A) Schematic diagram of complex formation strategy for ZBP (purple)-streptavidin (green) and biotin (red)-labeled DNA (orange) on ZnO nanowire (blue) array. (B) Kinetic binding of ZBP-streptavidin to ZnO nanowire array on a coverslip. Clustered ZnO NW array on a coverslip were incubated with 300 μg purified ZBP-streptavidin at 37°C for indicated time interval and the bound proteins were assessed by BCA protein assay kit (see Methods). (C and D) The electrophoretic mobility shift assay was performed to confirm the complex formation of ZBP-streptavidin and biotinylated DNA. Indicated amount of ZBP-streptavidin protein was incubated with biotinylated DNA encoding GFP expression cassette and the resulting complexes were 5 visualized under UV light after agarose gel electrophoresis (C). Relative binding of biotinylated DNA to ZBP-streptavidin was presented from triplicate experiments. Error bar, ± SD.

6.3.8. Role of nanowire penetration in gene expression

To link DNA molecules to ZnO nanowires, I utilized a ZBP-fused streptavidin and biotinylated DNA encoding expression cassette for green fluorescence protein (GFP) (Fig. 1-7). A fraction (~8%) of HEK293 cells incubated with FNW coated with ZBP–streptavidin and biotinylated DNA expressed GFP at 48 h after incubation, whereas GFP expression was barely observed in cells incubated with FNW only or FNW with free biotinylated DNA (Fig. 1-8). Expression of GFP in cells incubated with VNW complexed ZBP–streptavidin, and biotinylated DNA was not detected at all (data not shown).

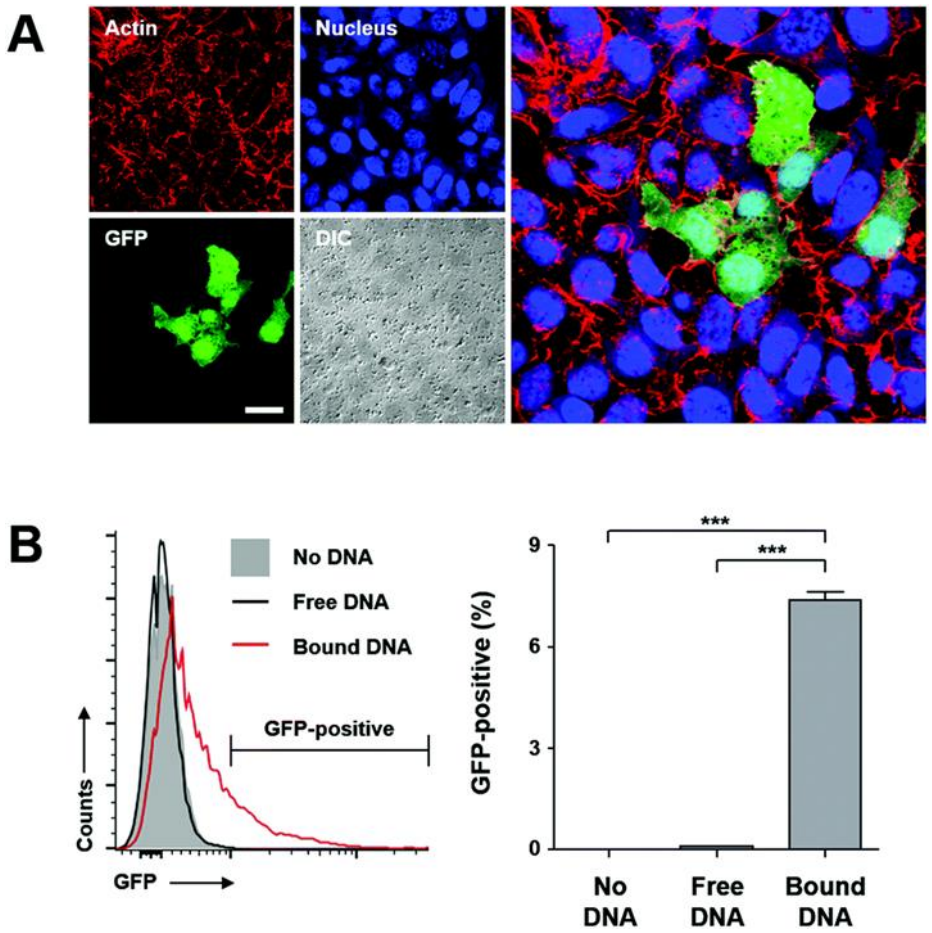

Figure 1-8. Intracellular delivery of DNA coated on clustered ZnO nanowire arrays. (A) Fluorescence image of HEK293 cells transfected with DNA encoding GFP-expression cassette. Cells were incubated on FNW arrays coated with linear DNA for 48 h and then stained with TO-PRO-3 and phalloidin for visualization of nuclei (blue) and the actin cytoskeleton (red), respectively. Excitation (ex.) and emission (em.) wavelengths for detecting the fluorescent probes by confocal microscopy are as follows; GFP: ex. 488 nm, em. 509 nm; Alexa Fluor 594-Phalloidin: ex. 581 nm, em. 609 nm; and

TO-PRO-3: ex. 642 nm, em. 661 nm. DIC: differential interference contrast, white bar: 10 μm. (B) FACS histograms showing GFP expression for different experimental groups. Percentile of GFP-positive cells was compared among the indicated experimental groups. Error bars indicate SD of experimental replicates ($n = 3$). ***, $p < 0.001$.

6.4. Discussion

Two types of 3 dimensional ZnO nanowire arrays were synthesized by a hydrothermal method and named them based on Morphology as vertical (VNW) and fan-shaped (FNW) nanowires. This Study has investigated potential Information of different physical conformation of the 3D ZnO nanowires with cellular responses, cytotoxicity as well as the efficacy of intracellular delivery of associated bio-macromolecules. Morphological features of FNW or VNW arrays in glass coverslips prepared on ZnO seed layer or ZnO nanoparticles, respectively, are presented in Fig 1-1. The diameter of ZnO nanowires range from 100 to 200 nm and the length are from 0.5 to 2.5 μm. X-ray diffraction patterns confirm the typical peaks of the wurtzite structure of ZnO crystal structures (Fig. 1-2).

In order to assess the cellular toxicity of ZnO nanowires, HEK293 cells were grown on VNW or FNW. The necrotic phenotypes may not be specific to ZnO nanowire arrays since normal glass coverslips also induced a similar degree of necrosis with the same time kinetics. It is also noteworthy that there was a subsequent rise in cellular necrosis between 24 and 48 h of incubation when cells were actively growing, indicating that physical damage causes cellular necrosis in a small fraction (<10%) of cells. Again, this minor rate of necrosis seems to be independent of ZnO nanowire arrays since normal glass coverslips also induced a similar degree of necrosis with similar time kinetics. Considering that cellular apoptosis gradually decreased during the exponential growth phase, the second rise in necrotic phenotype may reflect

physical damage to cellular membranes while cells start to rapidly grow in the new culture environment after the lag phase. Taken together, the degree of cell apoptosis, but not necrosis, was higher in the cells incubated on ZnO nanowire-coated coverslips than normal glass coverslips during the initial stage of incubation. Since cellular apoptosis was rapidly induced during the early phase (~6 h) of incubation with ZnO nanowire arrays and gradually declined thereafter, cellular adaptation potentially helps to overcome apoptotic stress endowed by ZnO nanowire contact while cells start to replicate on the foreign substrate. These findings provide interesting information on how cells respond and adapt to the inorganic nanowire substrate on glass coverslips. Although most of the current studies on inorganic nanowires have reported "minimal" toxicity based on viability and toxicity tests after the cells completely settle down and/or actively replicate on the nanowire structures (usually 24–48 h after incubation), our current findings on the differential kinetics of cellular apoptosis and necrosis in response to ZnO nanowire arrays underscore the importance of studying kinetics on cellular stress responses when cells are newly exposed to a foreign nanowire substrate.

Surface functionalization of nanowires is one of the essential factors to bind the biomolecules on the nanowire for any biological uses. Until now, alkoxysilanes has been widely used for the surface functionalization of nanowires, to bind biomolecules [48-49]. Here I have used previously reported Zinc oxide binding peptide for surface functionalization of nanowires [18, 47]. During imaging analysis, I observed close contact of cellular surfaces with ZBP-FITC-coated nanowires. Therefore, I next assessed the

intracellular delivery of the peptides coated on ZnO nanowires. As shown in Fig 1-6 A and 1-6 B, all the live cells collected after 30 min of incubation on ZBP-FITC-coated nanowire arrays were positive for FITC signal and the fluorescence intensities were saturated thereafter, albeit with slight fluctuations in signal intensities. These results indicate that the peptide molecules coated on the nanowires are efficiently and rapidly delivered into cells. Rapid saturation of the peptides also suggests that cells potentially uptake the peptide molecules coated on the tips of ZnO nanowires right after cellular contact. When I compared the morphological difference of 293t cells on FNW, VNW, and normal cover glass, I find out that the cells are trying to wrap FNW using filopodia (Fig. 1-5 C). Previously, it was shown that on SiO_2 nanopillars less than 300 nm in diameter and arranged at 1 μm intervals, the cell membrane wraps around the entirety of a nanopillar without the nanopillar puncturing the cell [25]. On the other hand, cells sit atop of arrays of larger, more closely spaced nanopillars [25]. Although our ZnO nanowires have a diameter of less than 200 nm, they are densely packed, so cells sit on VNW or wrap individual clusters of FNW via lamellipodia formation. Thus, cellular membranes mainly contact tips of ZnO nanowires (Fig. 1-5 D) and may rapidly take up peptides coating the tips of nanowires. These results support that FNW mediates more efficient physical penetration during the early contact period. Considering that FNW induced more cellular apoptosis than VNW during the early phase (~3 h) of incubation, without cellular necrosis in both ZnO nanowire arrays during this time frame (Fig. 1-3 C), the physical pressure exerted by the unevenly distributed FNW array might be more apoptogenic but insufficient to cause necrotic damage to cellular

membranes. In addition, the pressure imposed on cells by gravitation during FNW contact may allow for better intracellular access of the associated peptides than VNW contact at 4°C (Fig. 1-6 C-D).

Previously, two mechanisms of elastic cell membrane penetration have been proposed: "impaling penetration" as cells land onto a bed of nanowires and "adhesion-mediated penetration," which occurs as cells spread onto the substrate and generate adhesion force [50]. The difference in efficacy of intracellular delivery of the associated peptides on FNW and VNW at 4°C during the early phase (~ 30 min) of incubation might be due to the degree of impaling penetration since cellular spread on substrate is restricted at 4°C during the short incubation period (Fig. 1-6). Contact between cellular membrane and ZnO nanowire arrays potentially start from the tips of nanowires such that if nanowires are tilted or vertical, asymmetric elastic strain may affect subsequent contact [51-52]. The asymmetric contact of angled nanowires in FNW with cellular membrane may allow for better penetration of plasma membrane and actin cytoskeleton [53]. Transient penetration may occur shortly after seeding cells on the nanowire arrays and then further continued by lipid bilayer drift driven by surface tension [54]. The enhanced full penetration of the plasma membrane by FNW is further supported by the detectable gene expression of associated DNA (Fig. 1-9). In order to be expressed in eukaryotic cells, the DNA encoding an expression cassette must be delivered into the nucleus after passing through the plasma membrane. Since endocytosed molecules are generally delivered into lysosomes where cargo are degraded, GFP expression from delivered DNA demonstrates a direct penetration of the cellular membrane into nuclei by

FNW in a fraction (~ 8% in this study) of cells. Cellular penetration by FNW can be further intensified by cell-substrate adhesion tension during the initial contact phase, causing the cell membrane to spread onto the glass coverslip and deform toward the FNW (adhesion model). The full penetration of the plasma membrane, which is sufficient to mediate intracellular delivery of large DNA molecules, likely occurs at the apex of ZnO nanowires by the "tent-adhesion mechanism" during initial cell spreading [55]. It was shown that cellular penetration occurs rapidly within 30 min after seeding the cells on hollow nanowires and plateau after an extended period of time. Once cells engulf nanowires, cells do not further generate stress, thereby avoiding membrane failure [55-56].

Efficient intracellular delivery of biomacromolecules non-covalently associated with ZnO nanowires can be mediated by active cellular uptake, such as endocytosis, and/or direct penetration during the early phase of cellular contact. In addition, FNW might induce penetration of plasma membrane more efficiently than VNW, as evidenced by enhanced DNA transfection, but generates more apoptotic stress during the initial contact phase. Nevertheless, cells can survive and grow efficiently on both types of ZnO nanowire arrays with marginal toxicity after the initial lag phase. These results indicate that ZnO nanowire arrays could be an attractive nanomaterial for manipulating nano-bio interface with potential for further biomedical applications.

7. Chapter 2

Application of radially grown ZnO nanowires on poly-L-lactide microfibers complexed with a tumor antigen for cancer immunotherapy

7.1. Introduction

Zinc oxide (ZnO)-based nanocomposites have shown promising potential for various biomedical applications, including bioimaging, drug delivery, and vaccine development, due to its multifunctionality and biocompatibility [15, 18, 57]. Notably, it has been consistently shown that ZnO nanoparticles (NPs) possess adjuvant potential as vaccine carrier when combined with specific antigens [15, 18]. ZnO NP itself can exert immunomodulatory and inflammatory effects on antigen-presenting phagocytic cells (APCs), such as macrophages and dendritic cells [16, 59]. The immune-stimulatory function of ZnO nanocomposites might be due to induction of reactive oxygen species (ROSs), inflammatory cytokines, and cellular activation in APCs, which can link to antigen-specific adaptive immune responses, as well as intrinsic basal toxicity in vivo [36, 60]. It is notable that ZnO NP has the most drastic immunological effects in APCs among several inorganic NPs (TiO_2, TiO_2-silica, single-walled carbon nanotubes, and multi-walled carbon nanotubes) [61]. Moreover, surface modification of ZnO nanocomposites with specific peptides possessing a high affinity to the metal oxide composites also enables them to further enhance the antigen-specific adaptive immunity, including antibody and T cell responses in vivo [15, 18].

In the previous chapter, I also found that ZnO nanowires (NWs) can efficiently deliver associated biomacromolecules, including peptides and DNA, into eukaryotic cells if appropriately modified in a 3-dimensional conformation. It was also confirmed that radially grown “fan-shaped” ZnO nanowires (FNWs) on a coverslip can efficiently deliver the associated

peptides and DNA into eukaryotic cells via transient penetration of plasma membrane as well as cellular endocytosis, whereas delivery of the biomacromolecules on densely packed vertical ZnO nanowires (VNWs) might be primarily mediated by endocytosis with bare membrane penetration. Indeed, FNW can mediate intracellular delivery of DNA into the nucleus and its gene expression, confirming intracytoplasmic penetration crossover the cytoplasmic membrane, whereas VNW failed to do so. This phenomenon suggested that contact of angled nanowires with the plasma membrane and subsequent cellular spread can intensify membrane tension and induce transient penetration of plasma membrane, thereby enhancing the delivery into cytoplasm and nucleus. The delivery of an antigen into host cells, especially into APCs, is a critical step to determine antigen processing and presentation pathways to CD8 and CD4 T cells via MHC class I and II pathways [62]. Given that this two different antigen processing and presentation pathways are primarily dependent on antigen location in cellular cytoplasm and within intracellular vesicles, respectively, intracellular delivery of a protein antigen into cytoplasm may further enhance antigen-specific CD8 T cell responses mediated by MHC class I antigen presentation pathway, which can be efficiently linked to antigen-specific cytotoxic T lymphocyte (CTL) responses, critical players in anti-tumor immunity [34, 62- 64].

In this study, I investigated whether ZnO nanowires formed the unique 3-dimensional structure on poly-L-lactic acid (PLLA) microfibers, a biocompatible organic matrix, can induce a tumor antigen-specific CTL response and suppress tumor growth in vivo. Radially grown ZnO nanowires on PLLA fibers were complexed with a well-known tumor antigen,

carcinoembryonic antigen (CEA), fused with ZnO-binding peptide to exploit as a novel intracellular antigen delivery system [29]. I also confirmed the immune stimulatory effect of the inorganic-organic hybrid nanocomposites in vitro using phagocytic dendritic cell, a cellular bridge of innate and adaptive immunity [65]. Immunization with the CEA-coated hybrid nanocomposites can not only enhance the antigen-specific T cell responses but also suppress tumor growth significantly better than PLLA fibers mixed with CEA *in vivo* mouse model, demonstrating that incorporation of ZnO nanowires into the hybrid composite has promising potential as a vaccine adjuvant for antigen delivery as well as immune stimulation.

7.2. Material Methods

7.2.1. Synthesis of PLLA fiber-ZnO nanowire composites

PLLA microfiber-ZnO nanowire composites were synthesized as follows and supplied by Professor Young Keun Kim's laboratory, Korea University. Before the electrospinning process, the solution of PLLA polymer and ZnO nanoparticles (NPs) was prepared. Hexadecyltrimethylammonium bromide (CTAB) capped ZnO NPs with the size of 5 nm are synthesized by alkaline solution-based method according to a previous report. Then, PLLA (15 w/v %) polymer is dissolved in chloroform for several hours with magnetic stirring. The ZnO NP solution with the concentration of 10 mg/ml in ethanol is added to prepared PLA solution and mixed with vortex mixer and ultrasonication. The blended solution is injected into a 10 mL syringe which is mounted a 21-gauge metal needle tip with a diameter of 0.5 mm. A distance between needle and collector is adjusted to 10 cm. PLLA fiber-ZnO NP membranes are collected by electrospinning method with the applying voltage of 10 kV. Finally, PLA fiber-ZnO nanowires composites are synthesized via hydrothermal method for which the ZnO crystals are grown from ZnO NP embedded in PLLA fiber. 10 mM of zinc nitrate hexahydrate, ($Zn(NO_3)\cdot 6H_2O$) and 10 mM of hexamethylenetetramine (HMTA, $C_6H_{12}N_4$) are dissolved in deionized water to synthesize the ZnO nanowires on the PLLA fiber.

7.2.2. Characterization of PLLA fiber-ZnO nanowire

composites

The morphology and microstructure of the ZnO NPs and PLLA fiber-ZnO nanowires composites are analyzed using scanning electron microscopy (SEM, SU 70 Hitachi, Japan) at an accelerating voltage of 15 kV. The crystal structure and crystallite size of the samples are determined by measuring powder X-ray diffraction (XRD, PANalytical, X'Pert ProMPD) with Cu Kα radiation (λ = 1.5406 Å) with Cu Kα radiation (λ = 1.5406 Å). Measurements were conducted in θ–2 θ geometry from 30◦ to 60◦ at 45 kV and 40 mA tube power.

7.2.3. Mechanical fragmentation of PLLA fiber-ZnO nanowire composites

In order to mechanically fragment the composites, 10 mg of PLLA or PLLA-ZnO membranes were dispersed in dimethyl sulfoxide (DMSO) for 30 min and serially passed through ten times using a syringe with 18G, 23G, and 26G needles. The solution containing fragmented composites were then loaded on top of 80% sucrose solution and PLLA-ZnO nanocomposites were separated from PLLA fibers by density gradient centrifugation (3,515 x g, 30 min). The composites collected from the bottom layer were collected and further filtrated using 70 µm cell strainer (Sigma Aldrich, USA). The final fragmented PLLA-ZnO nanocomposites were washed with Phosphate-buffered saline (PBS) and used for further application. The size distribution of the fragmented complexes was measured by manually under the microscope. The procedure for fragmentation and separation of PLLA-ZnO

nanocomposites was summarized in Figure 2-2.

7.2.4. ZBP-FITC binding PLLA fiber-ZnO nanowire composites

Indicated amounts of ZnO-binding peptides (ZBP, amino acid sequences: RPHRKGGDARPHRKGGDARPHRKGGDA) labeled at their carboxyl terminals with fluorescein isothiocyanate (FITC, Peptron, Korea) were incubated with 250 μg of PLLA and PLLA-ZnO nanocomposite for 1 h at room temperature. The PLLA and PLLA-ZnO nanocomposites coated with ZBP-FITC were washed 3 times using PBS. This complex is resuspended in 100 μl of PBS, and then transferred to a 96 well black plate for fluorescence intensity measurement using Infinite®M200 PRO (Taken, Switzerland) or used for cell culture.

7.2.5. ZBP–CEA binding on PLLA fiber-ZnO nanowire composites

Different concentrations of ZBP–CEA were incubated with 250 μg of PLLA and PLLA-ZnO nanocomposites for 1 h at room temperature. The complex was washed 5 times using PBS. The bound proteins on PLLA and PLLA-ZnO nanocomposite were collected by centrifugation and quantitated by coomassie blue staining after SDS-PAGE.

7.2.6. Cellular uptake of ZBP-FITC coated on PLLA fiber-ZnO nanowire composites

PLLA and PLLA-ZnO nanocomposite were incubated with 6000 μM of ZBP-FTIC at room temperature for 1 h and washed 3 times using PBS to remove unbound peptides. Subsequently, this complex is incubated with DC2.4 at 37 ℃ for the indicated time. The cellular uptake of ZBP-FITC was examined after harvesting the cells using a flow cytometer (LSR II, BD Biosciences, USA).

7.2.7. Activation of DC2.4 cells cultured with PLLA fiber-ZnO nanowire composites

DC2.4 cells cultured PLLA and PLLA-ZnO nanocomposite s were washed with ice-cold FACS buffer (PBS containing 1% bovine serum albumin [BSA] and 1 mM EDTA) and blocked on ice for 30 min with ultra-block solution containing 10% rat sera, 10% hamster sera, 10% mouse sera (Sigma, USA), and 10 μg/ml of 2.4G2 monoclonal antibody (BD Pharmingen, USA). DC maturation was examined after staining with FITC-conjugated anti-I-Ab (clone AF6-120.1; BD Pharmingen, USA), PE-conjugated anti-CD40 (clone 3/23; BD Pharmingen, USA), APC-conjugated anti-CD80 (clone 16-10A1; eBioscience, USA), and PE/Cy7-conjugated anti-CD86 (clone GL-1; BioLegend, USA) for 30 min on ice. The cells were analyzed using a FACS (LSR II, BD Biosciences, USA) flow cytometer. Data were analyzed by FlowJo software version 8.8.6 (FlowJo, USA).

7.2.8. Viability of DC2.4 cells cultured with PLLA fiber-ZnO nanowire composites

DC2.4 cells were maintained in Roswell Park Memorial Institute medium (RPMI 1640) (Welgene, Korea) supplemented with 10% heat-inactivated fetal bovine serum (FBS) (Welgene, Korea), 100 U ml−1 penicillin, and 100 μg ml−1 streptomycin (Gibco BRL, USA) at 37°C in the presence of 5% CO2. The viability of the DC2.4 cells cultured with PLLA and PLLA-ZnO nanocomposite observed for 24 h by trypan blue staining and apoptosis assay. The cells were collected by trypsinization, and live cells were counted after trypan blue staining. Cellular apoptosis and necrosis were assessed after staining with annexin V-Alexa Fluor 488 (Biolegend, USA) and 7-aminoactinomycin D (7-AAD, (Biolegend, USA) using a flow cytometer (LSR II, BD Biosciences, USA) according to the manufacturer's instruction.

7.2.9. Cytokine analysis

Cytokines secreted in culture supernatants were analyzed by cytometric bead array using a Mouse Inflammation Kit (BD Biosciences, USA), according to the manufacturer's instructions. Culture media were changed before DC2.4 stimulation and the production of tumor necrosis factor (TNF) -α, IL-1β, IL-6, and IL-10 from stimulated DCs were measured at 18 h after incubation.

7.2.10. Intracellular cytokine staining

Lymphocytes collected from the spleen of immunized mice were cultured for 16 h in RPMI 1640 medium supplemented with 10% heat-inactivated FBS, 50 nM β–ME (Invitrogen), 100 units/ml penicillin-streptomycin, 2 mM L-glutamine (Welgene, Korea), and 20 μg/ml of purified CEA proteins in 24-well, flat-bottomed culture plates (5×10^6 cells/well). After incubation,

GolgiPlug (BD Biosciences, USA) was added for 6 h. Lymphocytes were washed three times with ice-cold FACS buffer. Cells were blocked with ultra-block solution for 30 min on ice and stained with BV-605 and Pe-cy7-conjugated CD4 and CD8 antibodies (BD Pharmingen, USA) for 30 min at 4°C. After surface CD4 or CD8 staining, cells were washed three times with ice-cold FACS buffer and subjected to intracellular cytokine staining using the Cytofix/Cytoperm kit according to the manufacturer`s instructions (BD Biosciences, USA). Intracellular interferon- (IFN-γ) was stained using an APC-conjugated anti-IFN-γ. XMG1.2; BD Pharmingen, USA) for 30 min at 4°C. The stained cells were analyzed with a FACS Canto II flow cytometer. Data were analyzed by FlowJo software version 8.8.6).

7.2.11. Cytotoxic T lymphocyte activity

Fourteen days after the second vaccination, splenocytes were harvested from the immunized mice and CTL assays were performed using a crystal violet/MTT absorbance assay as described previously [30]. CTLs were generated by stimulating the splenocytes with synthetic ZBPCEA peptide 16 h followed by incubation with MC38/CEA cells as a target for 24 h. After washing, the target cells were stained with crystal violet (4 mg/ml in PBS) for 30 min at room temperature. The plate was then washed with PBS and the cells lysed using methanol. Target cell survival was analyzed by measuring the absorbance at 570 nm.

7.2.12. Tumor growth and survival

C57BL/6 mice (Orient Bio, South Korea) were housed and maintained in the

specific pathogen-free facility at Seoul National University (SNU) College of Medicine. Animal experiments were performed after approval by the SNU IACUC (permission ID: SNU090805-5). Tumor-bearing mice were humanely sacrificed when tumors reached over 2 cm^3 at the day of observation. Six-week-old C57BL/6 mice were injected subcutaneously at the right flank with MC38/CEA cells (1×10^5 cells/mouse). At 7 d after tumor cell injection, the mice were immunized at the tail base with the indicated complex three times at weekly intervals. Five mice were used for each group. Tumors were measured by digital caliper (TESA SHOP-CAL, Willrich Precision, Switzerland). The tumor volume (mm3) was calculated as (A x B2)/2, where A is the long diameter, and B is the short diameter. Tumor-bearing mice were humanely sacrificed with CO_2 asphyxiation when tumors reached over 2 cm in diameter at the day of observation, and the surviving mice were monitored up to 30 days after tumor inoculation.

7.2.13. Isolation of tumor-infiltrating leukocytes

Tumor tissues obtained aseptically from mice and cut into fragments, washed twice with PBS, and then digested with an enzyme cocktail (DNase and Collagenase IV, Sigma Aldrich, USA) as described previously [86]. The resulting cell suspension was filtered through nylon mesh screens to remove cell clumps, washed three times with PBS and resuspended in ice-cold FACS buffer. The tumor-derived cell mixtures were used for FACS analysis.

7.3. Results

7.3.1. Characterization and fragmentation of PLLA fiber-ZnO composites

Characteristic features of synthesized PLLA fiber-ZnO nanowire composites are presented in Fig. 2-1. As shown in scanning electron microscopy (SEM) images, ZnO nanowires are grown uniformly on the PLLA fibers. The diameter of PLA fiber is 1.25 μm in average. After 2 h of hydrothermal reaction, the ZnO nanowires have a diameter of 122.5 ± 4 nm, and a length of 1,375 ± 247 nm. We measure the XRD patterns to analyze the crystal structures of the composites. The diffraction peaks in Figure 2-1 B are appeared at 31.8°, 34.4°, 36.3°, 47.5°, 62.8°, and 67.7°, which can be assigned to (100), (002), (101), (102), and (110) planes of the ZnO nanowires with hexagonal closed packed (hcp) structure (PDF no. 36-1451), respectively. The diffraction peaks of ZnO nanowires become sharp as ZnO nanowires are grown from ZnO NPs. In order to obtain injectable forms of PLLA fiber-ZnO nanowires composites for in vivo application, I fragmented and collected the PLLA fiber-ZnO nanowires composites by density gradient centrifugation after mechanical shearing in DMSO solution using a syringe with 18G, 23G, and 26G needles (Fig. 2-2). Approximate Sizes of the fragmented composites range 1 ~ 70 μm in diameter with average of 15 μm (Fig. 2-2).

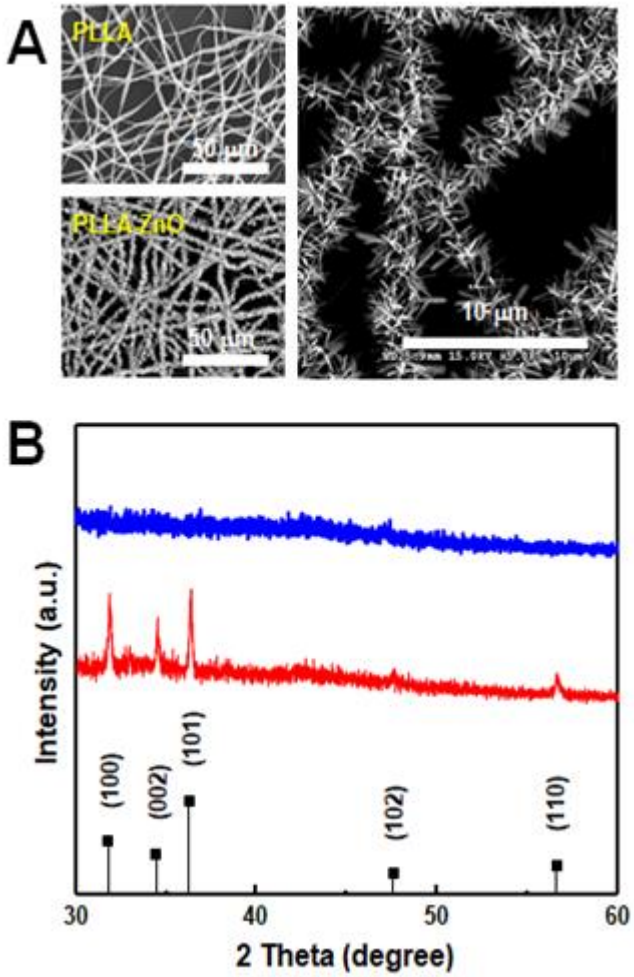

Figure 2-1. Morphological and microstructural analysis of PLLA fibers and PLLA fiber-ZnO nanowires composites. (A) SEM images of PLLA fibers (top left) and PLLA fiber-ZnO nanowires composites (left bottom and right with different magnifications). (B) XRD patterns of PLLA fiber (blue), PLLA fiber-ZnO nanowires composite (red). The ZnO peak positions are denoted in the bottom of the panel by the black vertical line.

7.3.2. Effect of PLLA fiber-ZnO nanowire composites on cell viability

In order to assess the cellular toxicity of PLLA fiber-ZnO nanowires composites, DC2.4 cells were treated with the nanocomposites, and live cell counts were compared with untreated control cells or PLLA fiber-treated cells (Fig. 2-3). Live cell counts gradually increased in the cultures after 6 h of lag phase, indicating that DC2.4 cells can replicate in the presence of PLLA fiber-ZnO nanowires composites, albeit with lower growth rates than those of untreated cells or PLLA fiber-treated cells (Fig. 2-3 A). To assess for potential toxicity during the lag phase, I examined cellular necrosis and apoptosis (Fig. 2-3 B and 2-3 C). Apoptotic cell death was gradually increased up to 12 h after incubation with PLLA fiber-ZnO nanowires composites, suggesting that cellular apoptosis is induced in a fraction of cells by treatment of PLLA fiber-ZnO nanowires composites, and then decreased to normal range, comparable to those of untreated or PLLA fiber-treated cells in 24 h after incubation. Even though induction of apoptosis was also observed in cells treated with PLLA fibers, ZnO nanowires might be responsible for enhanced apoptotic cell death. Cells treated with PLLA fiber-ZnO nanowires composites showed similar degree (4.1 ~ 5.3%) of early apoptotic phenotype when compared to those (4.1 ~ 5.5%) treated with PLLA fibers up to 24 h of incubation. However, late apoptotic cells positive for both 7-aminoactinomycin D (7-AAD) and annexin V peaked (~ 25.5%) at 12 h after incubation in cells treated with PLLA fiber-ZnO nanowires composites, whereas they were observed in significantly lower degree (4.7 ~ 14.5%) when treated with PLLA fibers throughout the incubation period. Interestingly, necrotic cells were barely detected (generally

less than 2.0%) in all the experimental groups, suggesting direct physical damages, as measured by membrane penetration of 7-AAD without annexin V staining, on cells exerted by PLLA fibers or by ZnO nanowires might be negligible.

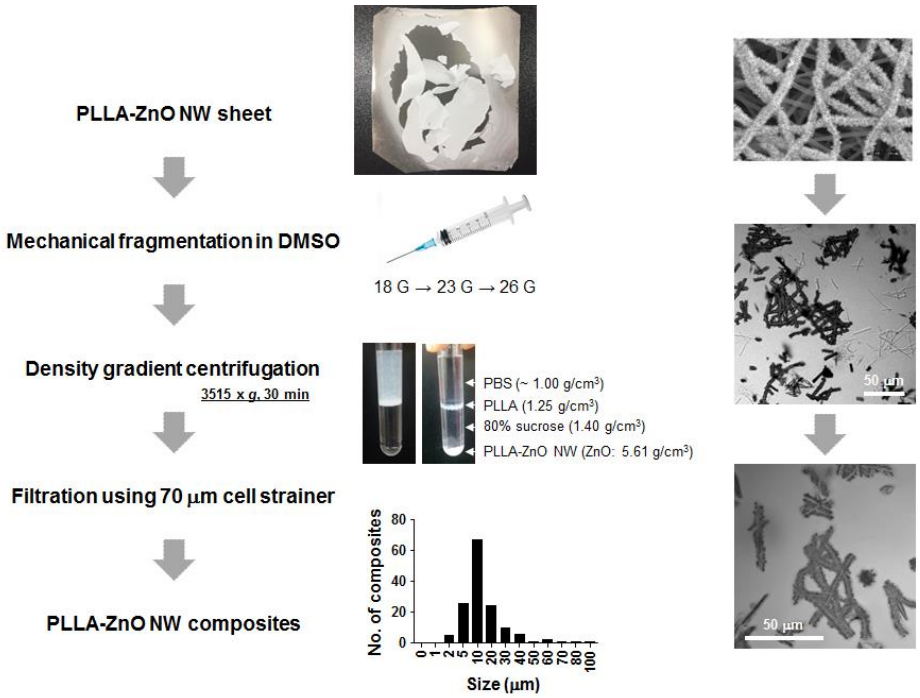

Figure 2-2. Schematic diagram and representative images of steps for preparation of PLLA-ZnO nanowires composites.

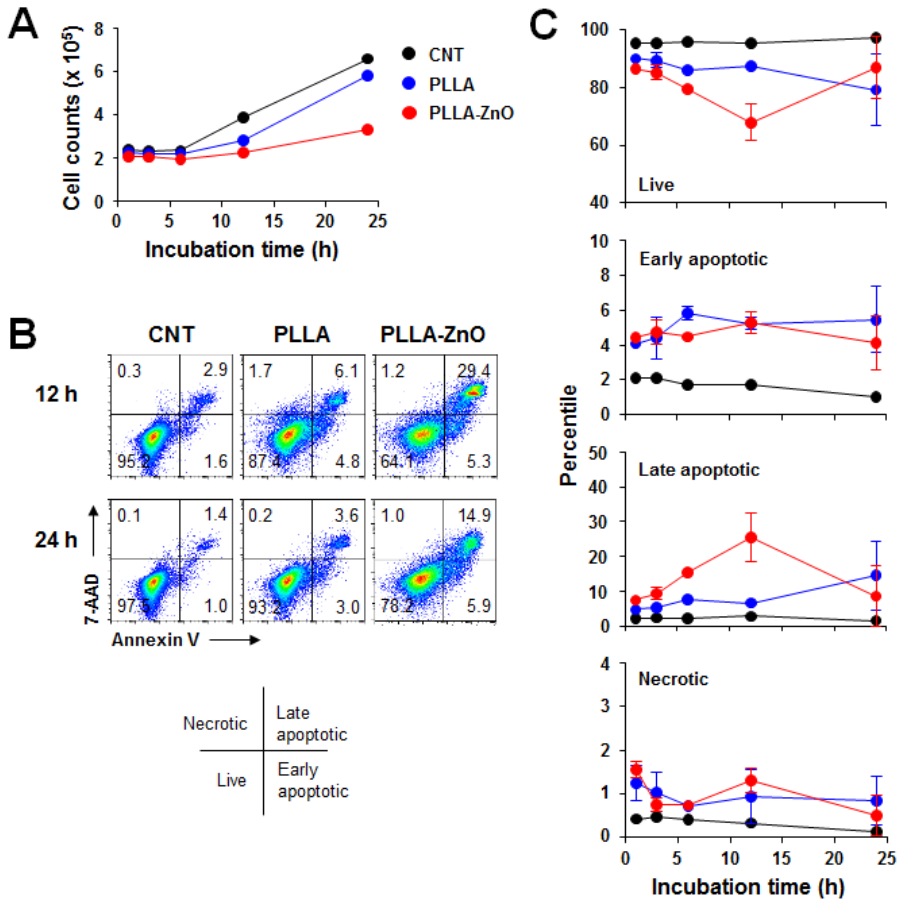

Figure 2-3. The effect of PLLA fiber-ZnO nanowires composites on cell viability. (A) DC2.4 cells were grown in the absence (CNT) or presence of 250 μg of PLLA fibers (PLLA) or PLLA fiber-ZnO nanowire composites (PLLA-ZnO), and their growth was monitored for up to 24 h. (B and C) Cellular apoptosis and necrosis were assessed by flow cytometry after annexin V and 7-AAD staining at the indicated times after cell culture

7.3.3. Binding of antigen with PLLA fiber-ZnO nanowire composites

In order to utilize PLLA fiber-ZnO nanowire composites as an antigen delivery system, I used a ZnO-binding peptide (ZBP) and examined its binding capacity to the nanocomposites (Fig. 2-4). The binding of ZBP-FITC to PLLA fiber-ZnO nanowire composites was assessed at titrated concentrations of ZBP-FITC after incubation for 1 h and then measured by fluorescence intensities and fluorescent microscopy (Fig. 2-4 A-B). ZBP-FITC was saturated at ~3.2 μM with 250 μg of PLLA fiber-ZnO nanowire composites. Although the peptide can bind nonspecifically to PLLA fibers and was saturated at the same peptide concentration, the amount of bound peptides was approximately one-third of those bound to PLLA fiber-ZnO nanowire composites, as measured by fluorescence intensity (Fig. 2-4 B). Next, I used recombinant carcinoembryonic antigen (CEA) fused with 3× ZBP as a model antigen to investigate the applicability of the nanocomposites for cancer immunotherapy. Consistently, ZBP-CEA showed enhanced binding to PLLA fiber-ZnO NANOWIRES composites when compared with PLLA fibers (Fig. 2-4 C-D). Approximately 22 μg of ZBP-CEA protein showed saturated binding to 250 μg of PLLA fiber-ZnO nanowire composites, whereas 15 μg of ZBP-CEA was saturated with the same amount of PLLA fibers when incubated them with 80 μg of the antigen for 1 h. Non-specific adsorption of a protein, ovalbumin, has also been reported previously.

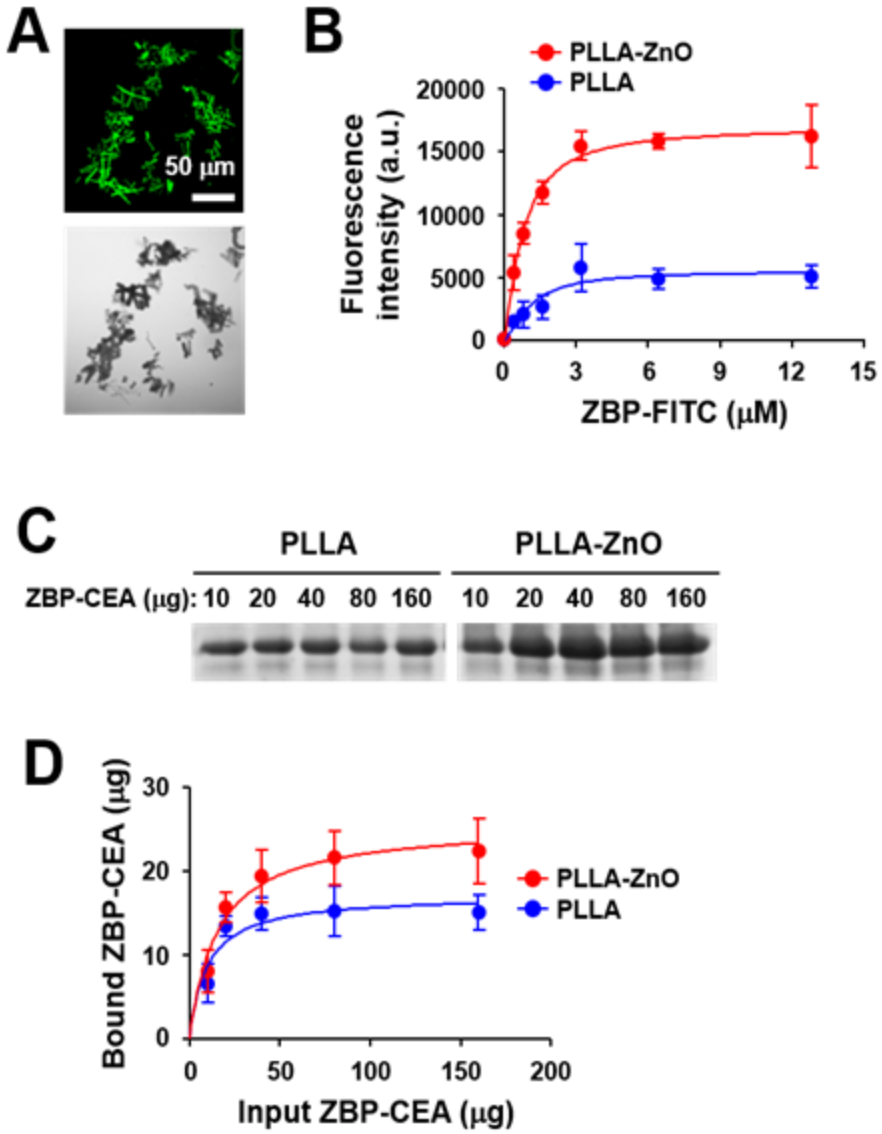

Figure 2-4. Immobilization of polypeptide on PLLA fiber-ZnO nanowire composites. (A) Microscopic image of fragmented PLLA fiber-ZnO nanowire composites coated with ZBP-labeled with FITC. Representative fluorescence (top) or differential interference contrast (bottom) images of the

nanocomposite fragments are presented. (B) Indicated amounts of ZBP-FITC were incubated with the composites (250 μg) at room temperature for 1 h, and the relative binding of ZBP-FITC was assessed by measuring the fluorescence intensity. a.u., arbitrary unit. The data are from three separate experiments. (C) Gel electrophoresis data showing the relative fraction of bound CEA antigen to PLLA fibers (PLLA) or PLLA fiber-ZnO nanowire composites (PLLA-ZnO). Bound CEA was resolved by sodium dodecyl sulphate polyacrylamide gel electrophoresis after incubation with the composites (250 μg) and the indicated amounts of CEA. (D) Bound CEA amount from (C) were quantitated from three separate experiments and presented.

7.3.4. Intracellular antigen delivery by PLLA fiber-ZnO nanowire composites

Next, I assessed the efficacy of intracellular delivery of the associated antigen into dendritic cells by using the composites, since I previously observed efficient delivery of biomacromolecules coated on the surface of radially grown ZnO nanowires into eukaryotic cells. As shown in Fig 2-5 A and B, most (> 90%) of the live cells collected after 30 min of incubation at 37°C on ZBP-FITC-coated PLLA fiber-ZnO nanowire composites were positive for FITC signal, and the fluorescence intensities were saturated thereafter, whereas only a fraction (~ 35%) of DC2.4 cells incubated with equal amount of PLLA fiber mixed with ZBP-FITC showed positive signals for FITC after 30 min of incubation and the positive percentile was rapidly declined to ~ 10% thereafter.

7.3.5. Effect of PLLA fiber-ZnO nanowire composites on DC2.4 cell activation

I measured inflammatory cytokines secreted by DC2.4 cells after stimulation with PLLA fiber-ZnO nanowire composites. Treatment of the nanocomposites induced significantly higher levels of inflammatory cytokines, such as IL-1β, IL-6, IL-10, and TNF-α when compare with untreated or PLLA fiber-treated cells, although the cytokine responses, except TNF-α, were generally lower in cells stimulated with LPS as a positive control (Fig. 2-6). Nevertheless, all the cytokine levels, except IL-1β, were further elevated in cell culture supernatants from cells treated with the PLLA fiber-ZnO nanowire

composites when compared to those from PLLA fiber-treated cells, suggesting that ZnO nanowires might be the primary stimulatory components to enhance the inflammatory responses in dendritic cells.

To further confirm the cellular activation, the activation markers of dendritic cells were also examined after stimulation with the nanocomposites. The surface expression of the activation markers, CD40 and CD80, were significantly increased after stimulation with PLLA fiber-ZnO nanowire composites when compared to those of untreated cells (Fig. 2-7 A-B), whereas expression of MHC II and CD86 on the DC2.4 cells was only slightly increased without statistical significance (Fig. 2-7 B). None of the activation markers was significantly elevated in cells treated with PLLA fibers, suggesting again that ZnO nanowires might be primary stimulants for the cellular activation, even though the degree of activation was generally lower than those stimulated with LPS.

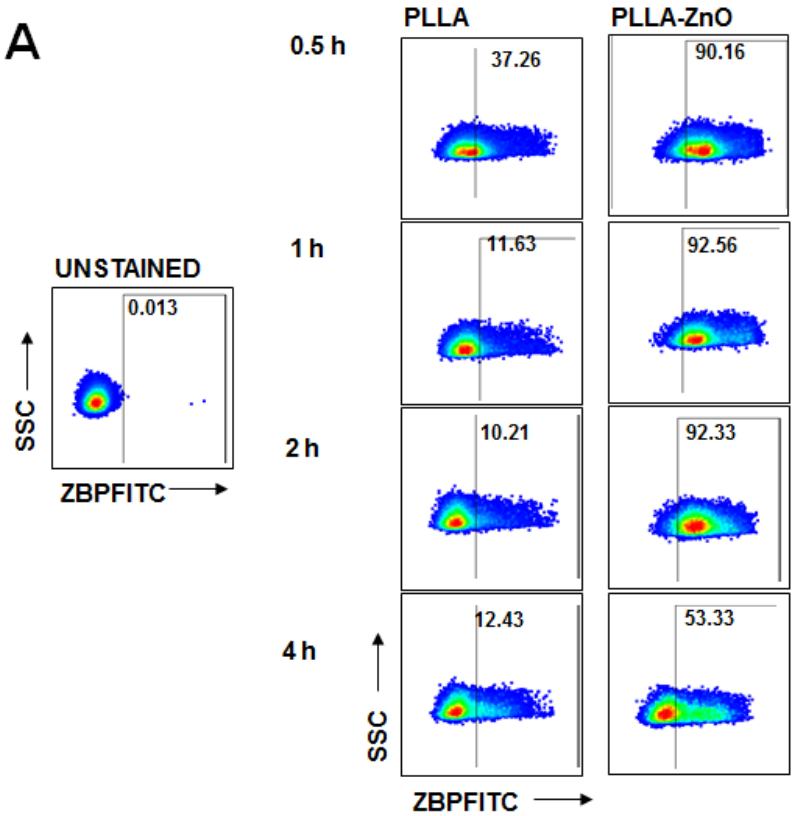
A
PLLA
PLLA-ZnO
0.5 h
1 h
2 h
4 h
37.26
90.16
11.63
92.56
10.21
92.33
12.43
53.33
UNSTAINED
0.013
SSC
ZBPFITC

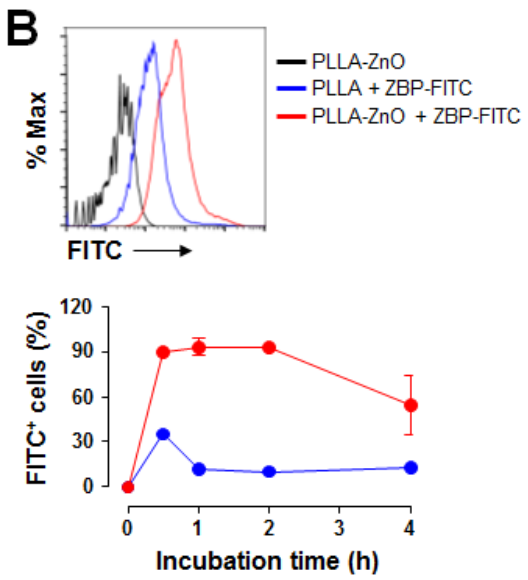
B
% Max
FITC
PLLA-ZnO
PLLA + ZBP-FITC
PLLA-ZnO + ZBP-FITC
FITC+ cells (%)
120
90
60
30
0
0
1
2
3
4
Incubation time (h)

Figure 2-5. Intracellular uptake of peptides coated on PLLA fiber ZnO nanowire composites by dendritic cells.

DC2.4 cells were incubated with indicated complexes coated with ZBP-FITC at 37°C for the indicated times and analyzed by flow cytometry. (A) Live cells were gated based on a scatter plot, and fluorescence intensities of cells were assessed. Representative flow cytometric data and the kinetic changes of FITC-positive cellular fraction are presented. (B) Representative histograms of the indicated cell subset cultured with PLLA or PLLA-ZnO nano composite. The graphical representation of saturation percentage of fluorescein positive-stained cells at different time points. Diagrams show the mean percentage of fluorescein-positive cells of triplicate samples.

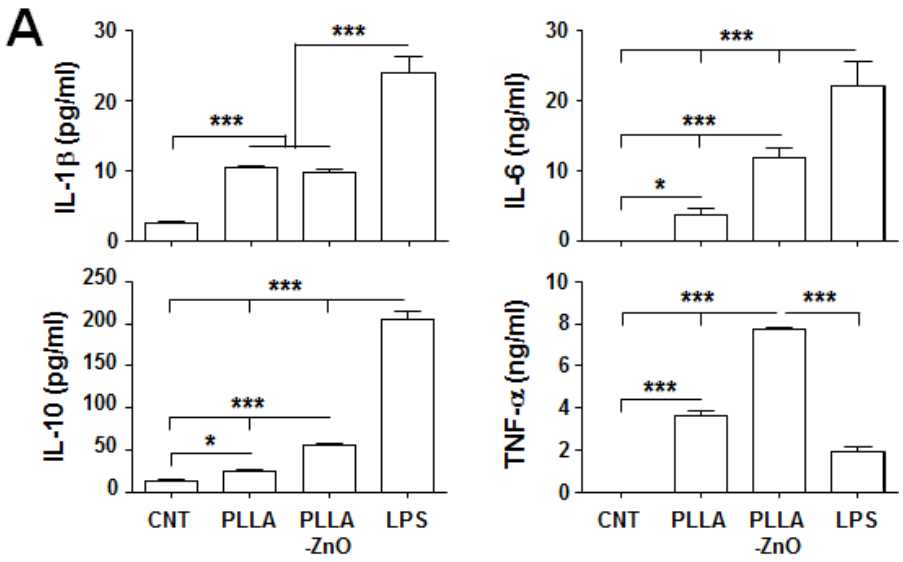

Figure 2-6. Pro-inflammatory response of dendritic cells cultured with PLLA fiber-ZnO nanowire composites. DC2.4 cells were incubated with the indicated complexes at 37°C for 18 h and inflammatory cytokines were measured in the culture supernatants ($n = 4$). $p < 0.05$; **, $p < 0.01$; ***, $p < 0.001$.

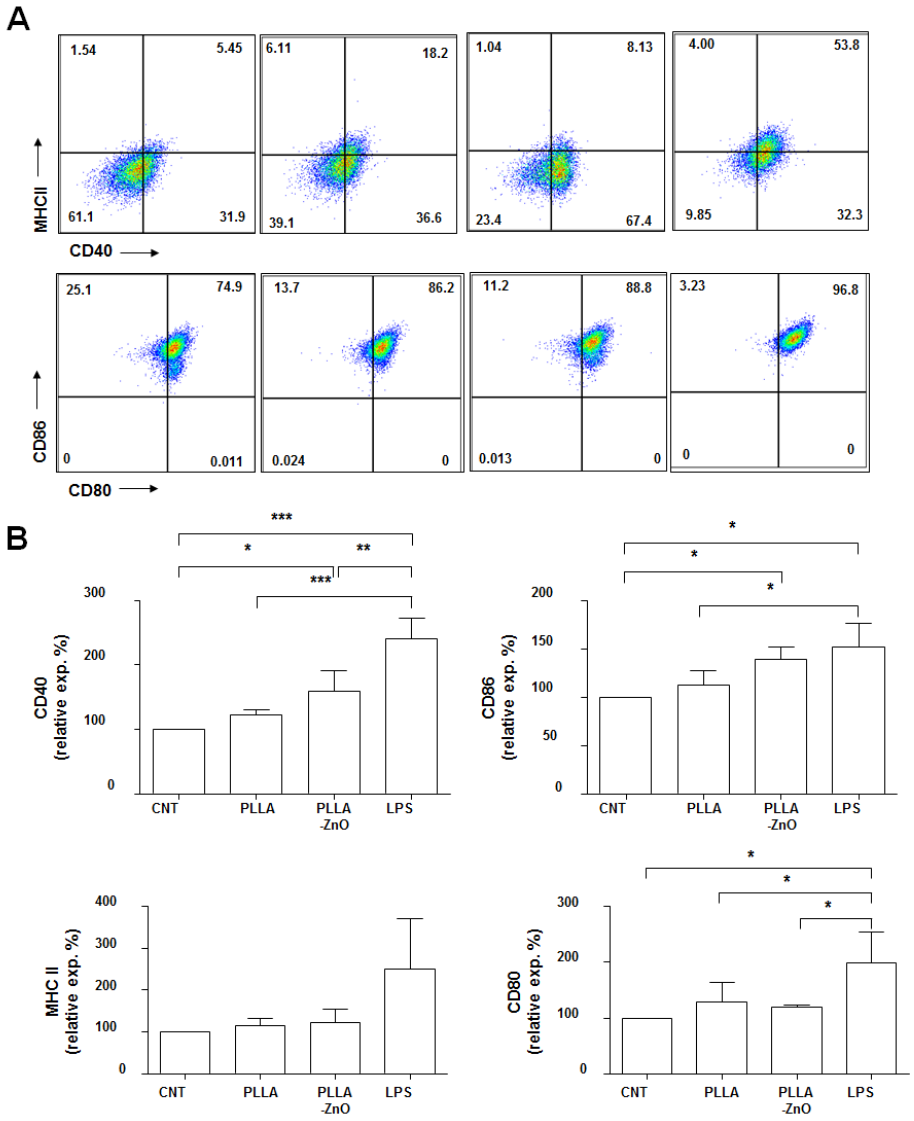

Figure 2-7. Effect on surface expression of the co-stimulatory molecule in dendritic cells cultured with PLLA fiber-ZnO nanowire composites.

Phenotypic changes of DC2.4 cells after stimulation with the indicated complexes were examined by staining for cellular surface markers. (A) The

surface expressions of the co-stimulatory molecules on DC2.4 cells were analyzed by flow cytometry. (B) The relative surface expression levels of indicated molecules in comparison with untreated cells (CNT) were presented ($n = 4$). *, $p < 0.05$; **, $p < 0.01$; ***, $p < 0.001$.

7.3.6. T cell responses induced by PLLA fiber-ZnO nanowire composites

I directly immunized C57BL/6 mice with PLLA fiber-ZnO nanowire composites (1 mg/mouse) mixed with 100 μg of ZBP-CEA and analyzed CEA-specific cellular immunity. At two weeks after second immunization, I examined T-cell responses in splenocytes by measuring their production of IFN-γ, a hallmark cytokine for cell-mediated immunity, in an antigen-dependent manner (Fig. 2-8 A). The frequencies of IFN-γ-secreting CD4 or CD8 T cells in spleens of mice immunized with the nanocomposites complexed with ZBP-CEA significantly increased, when compared to those of non-immunized controls (CNT and PLLA-ZnO) or mice immunized with PLLA fibers mixed with the same amount of ZBP-CEA antigens. It is notable that presence of ZnO nanowires in the complex significantly enhanced the antigen-specific T cells responses by approximately 70 ~ 100%. Furthermore, prominent cytotoxic responses against CEA-expressing cancer cells (MC38/CEA) were induced in mice immunized with the nanocomposites complexed with ZBP–CEA, whereas no significant cytotoxicity was detected in the control groups (Fig. 2-8 B), PLLA-ZnO only or untreated group [data not shown].

7.3.7. Anti-cancer effect of PLLA fiber-ZnO nanowire composites

To further prove the functional significance of CEA-specific adaptive

immunity generated in vivo for anti-cancer immunotherapy, mice inoculated with MC38/CEA cells were immunized three times with weekly intervals and the tumor growth was monitored for a month. As shown in Fig 2-8 C, tumor growth was significantly suppressed in mice immunized with PLLA fiber-ZnO nanowire composites coated with ZBP–CEA and all of them survived, whereas other control groups failed to protect the mice during the observation period and all the mice were sacrificed due to the enlarged tumors. Since we observed mice immunized with PLLA fibers mixed with ZBP-CEA also showed significance rise of CEA-specific T cell responses, but failed to suppress the tumor growth. The systemic immunosuppression and the infiltration of T cells in growing tumors were assessed at day 24 after tumor inoculation in the immunized mice groups by analyzing the proportion of T cells in spleens and tumors, respectively (Fig. 2-9 and 2-10). Systemic reductions of T cells, as well as gradual increase in regulatory T cells (T_{reg}) in tumor-bearing hosts, have been well established. In addition, immune contextures of growing tumors, especially tumor-infiltrating CTLs, have been shown to correlate with clinical outcomes [74]. In spleens of tumor-bearing mice, I observed drastic reduction of CD4 and CD8 T cells, generally less than 1 and 2 % among whole splenocytes, respectively (Fig. 2-9).

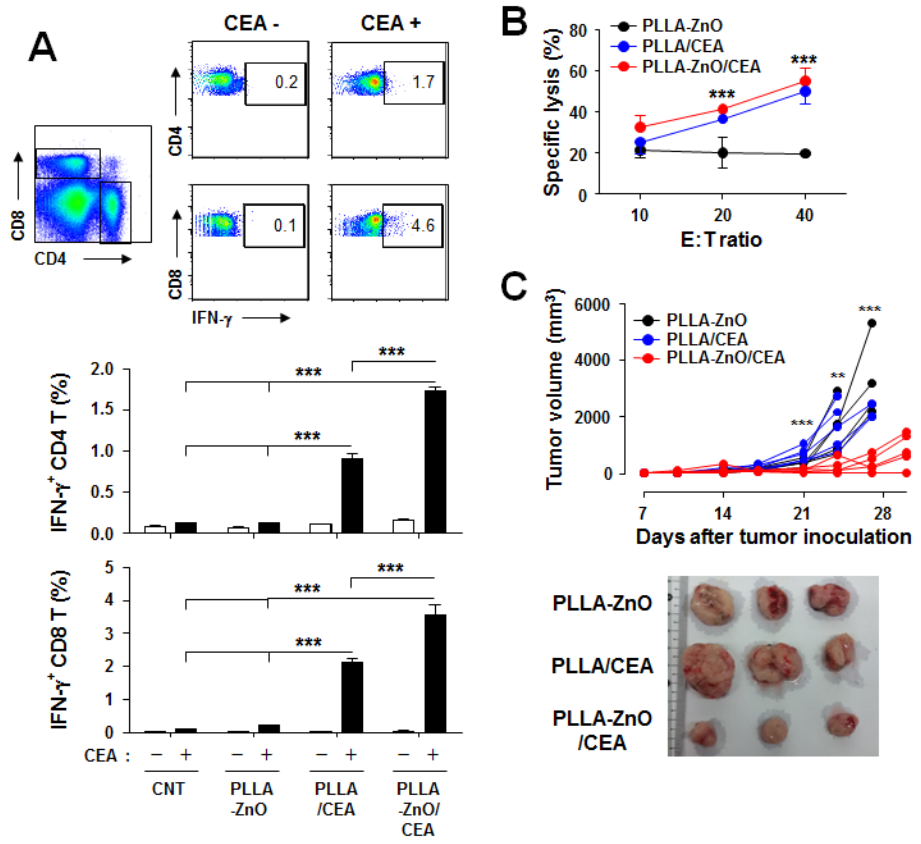

Figure 2-8. CEA-specific, IFN-γ-positive CD4 and CD8 T-cell responses of mice immunized with the indicated complexes. (A) IFN-γ-positive T cells in splenocytes were detected in the presence (+) or absence (–) of CEA. Top panels: representative dot plots. Bottom panels: average percentiles of the T cells from three independent experiments. (B) Cytotoxic activity of splenocytes from immunized mice. MC38 cells expressing CEA (MC38/CEA) were used as targets. (C) Tumor volume of mice (5 mice/group) injected with MC38/CEA cells. Mice were immunized three times with the indicated complexes at 7, 14, 21 days after tumor cell injection. Mice bearing

tumors over 2 cm^3 at the day of observation were sacrificed humanely. Representative images of tumors collected from sacrificed mice (bottom picture, tumors from PLLA-ZnO/CEA group at day 30). **, $p < 0.01$; ***, $p < 0.001$.

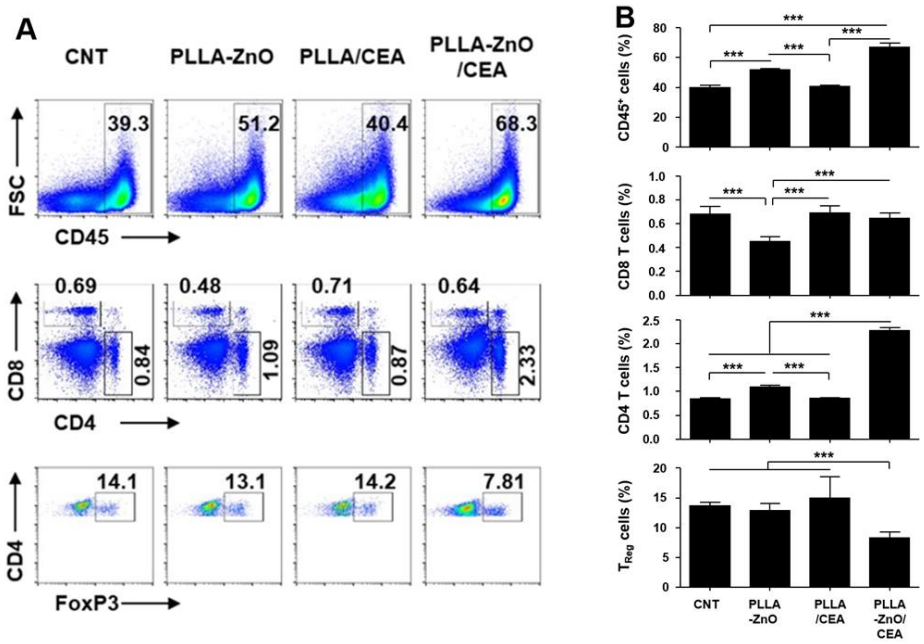

Figure 2-9. Flow cytometry analysis of immune cells subsets in spleen of tumor bearing mice. Hematopoietic immune cells were quantitated in spleen at day 24 after tumor inoculation in the indicated mice groups. (A) Gating strategy for relative fraction of hematopoietic immune cells in spleen. (B) Relative fractions *(n = 3)* of hematopoietic immune cells ($CD45^+$), $CD4^+$, $CD8^+$, and regulator T cells ($T_{reg,}$ $CD4^+/FoxP3^+$). CNT: non-immunized mice. *, $p < 0.05$; **, $p < 0.01$; ***, $p < 0.001$.

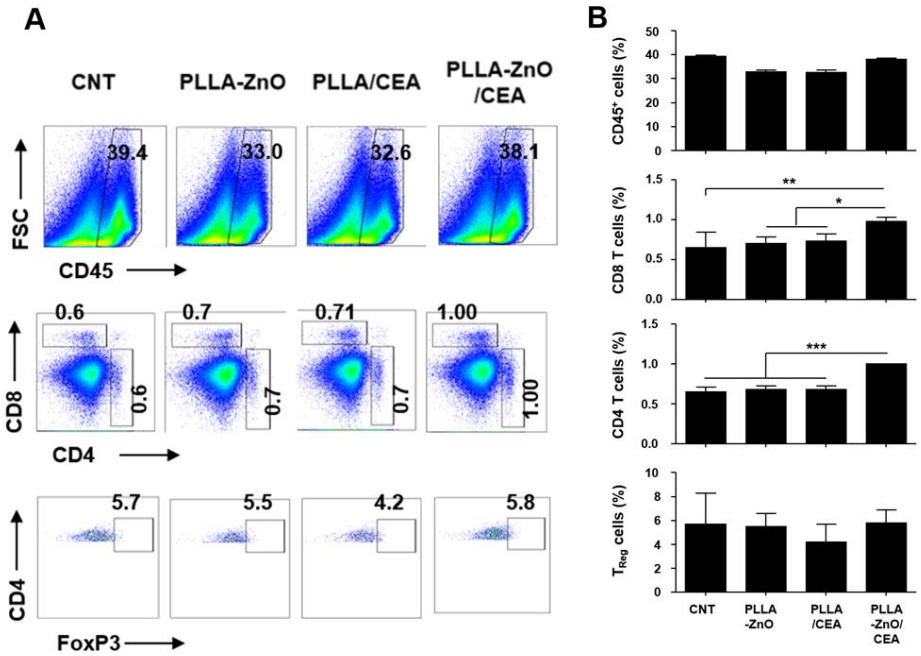

Figure 2-10. Flow cytometry analysis of tumor infiltrating immune cells subsets in tumor tissues. ($CD45^+$), $CD4^+$, $CD8^+$, and regulator T ($T_{reg,}$ $CD4^+/FoxP3^+$) cells were quantitated in tumor tissues at day 24 after tumor inoculation in the indicated mice groups (A) Representative flow cytometric plots showing progressive gating strategy for analysis of tumor infiltrating lymphocytes. (B) Relative fractions *(n = 3)* of tumor infiltrating immune cells. CNT: non-immunized mice. *, $p < 0.05$; **, $p < 0.01$; ***, $p < 0.001$.

7.4. Discussion

It has been shown that ZnO nanowires can be grown as radial bundles from ZnO NPs which are dispersed in solution or coated outside of various kinds of substrates [83-84]. However, it is interesting to note that we can obtain similar morphology of ZnO nanowires to the previous reports even if the seed layer of ZnO NPs exist inside the PLLA fibers. The precursors dissolved in the aqueous solution such as Zn^{2+} and OH- may diffuse into PLLA fiber during the hydrothermal reaction, and the ZnO crystals can be gradually nucleated and grown as radial nanowires on the surface of ZnO NPs, potentially exposed on PLLA fibers, serving as seeds. The kinetic responses of cellular apoptosis induced by PLLA fiber-ZnO nanowire composites were slightly different from those observed in the previous study using ZnO nanowire arrays on glass coverslip. HEK293 cells grown on glass coverslips coated with ZnO nanowires showed early apoptotic phenotype peaked (~ 40%) at the earlier stage (~3 h) of exposure and late apoptosis were peaked (~ 35%) at 6 h of incubation. This might be due to the cell type differences (phagocytic dendritic cell vs. fibroblast) or the culture matrix (plastic culture plate vs. glass cover slip). Nevertheless, the degree of cellular apoptosis, but not necrosis, was significantly higher in both of the cell types, primarily due to ZnO nanowires, during the initial stage of incubation. Since cellular apoptosis was rapidly induced during the early phase of incubation with ZnO nanowires and gradually declined thereafter, cellular adaptation potentially helps to overcome apoptotic stress endowed by ZnO nanowires and cells can start to replicate even in the presence of the ZnO nanowire composites, as

consistently observed in our previous and current studies.

To utilize PLLA fiber-ZnO nanowire composites as an antigen delivery system, we used a ZnO-binding peptide (ZBP) and examined its binding capacity to the nanocomposites. Approximately 22 μg of ZBP-CEA protein showed saturated binding to 250 μg of PLLA fiber-ZnO nanowire composites, whereas 15 μg of ZBP-CEA was saturated with the same amount of PLLA fibers when incubated them with 80 μg of the antigen for 1 h (Fig. 2-4). Non-specific adsorption of a protein, ovalbumin, has also been reported previously [85]. Nevertheless, these results show that the tumor-associated protein antigen fused with ZBP could be immobilized more efficiently on the PLLA fiber-ZnO nanowire composites than unmodified PLLA fibers, primarily via enhanced affinity to ZnO nanowires endowed by conjugated ZBP [15, 18]. In addition, the larger surface area of ZnO nanowires may enhance the binding capacity of the nanocomposites over the naked PLLA fiber. Next, I accessed the efficacy of intracellular delivery of the associated antigen into dendritic cells by using the composites coated with FITC antigen, since in previous chapter efficient delivery of biomacromolecules coated on the surface of radially grown ZnO nanowires into eukaryotic cells was observed. A very high percentage (> 90%) of the live cells collected after 30 min of incubation at 37°C on ZBP-FITC-coated PLLA fiber-ZnO nanowire composites were positive for FITC signal compared to PLLA fiber (Fig. 2-5 A-B). These results indicate that the peptide molecules coated on the nanowires are efficiently and rapidly delivered into the antigen-presenting cells. Rapid saturation of the peptides also suggests that cells potentially uptake the peptide molecules coated on the tips of ZnO nanowires right after

cellular contact, as observed in the previous study.

Since we and others consistently observed immunomodulatory and/or inflammatory effects of ZnO nanostructures on antigen-presenting phagocytic cells, including macrophages and dendritic cells [15, 21, 61, 66]. I measured inflammatory cytokines secreted by DC2.4 cells after stimulation with PLLA fiber-ZnO nanowire composites. A significantly higher level of inflammatory cytokines, such as IL-1β, IL-6, IL-10, and TNF-α was observed, although the cytokine responses, except TNF-α, were generally lower in cells stimulated with LPS as positive control (Fig. 2-6). However, these cytokine responses, except TNF- α, were generally lower in cells stimulated with LPS as positive control. Nevertheless, all the cytokine levels, except IL-1 β, were further elevated in cell culture supernatants from cells treated with the PLLA fiber – ZnO nanowires composites, when compared to those from PLLA fiber-treated cells, suggesting that ZnO nanowires might be the primary stimulatory components in enhancing inflammatory responses in dendritic cells.

To further confirm cellular activation of dendritic cells, I examined activation markers after stimulation with the nanocomposites. The surface expression of the activation markers, CD40 and CD80, were significantly increased after stimulation with PLLA fiber-ZnO nanowire composites when compared to those of untreated cells (Fig. 2-7), while expression of MHC II and CD86 on the DC2.4 cells was only slightly increased without statistical significance (Fig. 2-7 A-B). None of the activation markers was significantly elevated in cells treated with PLLA fibers, suggesting that ZnO nanowires might be primary stimulants for the cellular activation, even though the degree of activation was generally lower than those stimulated with LPS. None of the

activation markers was significantly elevated in cells treated with PLLA fibers, suggesting again that ZnO nanowires might be primary stimulants for the cellular activation, even though the degree of activation was generally lower than those stimulated with LPS. These results demonstrate that PLLA fiber-ZnO nanowire composites can stimulate the antigen presenting phagocytes and induce inflammatory responses, primarily due to ZnO nanowire components. Significant induction of the inflammatory cytokines, as well as activation of dendritic cells, by PLLA fiber-ZnO nanowire composites, prompted me to examine potential applicability of the nanocomposites as an immune-adjuvant for cancer immunotherapy. T-cell responses in splenocytes by measuring their production of IFN-γ, a hallmark cytokine for cell-mediated immunity, in an antigen-dependent manner, were examined. The frequencies of IFN-γ-secreting CD4 or CD8 T cells in spleens of mice immunized with the nanocomposites complexed with ZBP-CEA significantly increased. It is notable that the presence of zno nanowires in the complex significantly enhanced the antigen-specific T cells responses by approximately 70 ~ 100%. Furthermore, prominent cytotoxic responses against CEA-expressing cancer cells (MC38/CEA) were induced in mice immunized with the nanocomposites complexed with ZBP–CEA, whereas no significant cytotoxicity was detected in the control groups (Fig. 2-8 B). Even though splenocytes from mice immunized with PLLA fiber mixed with ZBP-CEA also enhanced the cytotoxic activity against the cancer cells expressing CEA, those from mice immunized with the nanocomposites coated with the cancer antigen always showed slightly better CTL activity, but without statistical significance (Fig. 2-8 B). To further prove the functional

significance of CEA-specific adaptive immunity generated *in vivo* for anti-cancer immunotherapy, mice inoculated with MC38/CEA cells were immunized three times with weekly intervals and the tumor growth was monitored for a month. It was observed that tumor growth was significantly suppressed in mice immunized with PLLA fiber-ZnO nanowire composites coated with ZBP–CEA and all of them survived, whereas other control groups failed to protect the mice. Since we observed mice immunized with PLLA fibers mixed with ZBP-CEA also showed significance rise of CEA-specific T cell responses, but failed to suppress the tumor growth, systemic immunosuppression and the infiltration of T cells in growing tumors were assessed at day 24 after tumor inoculation in the immunized mice groups by analyzing the proportion of T cells in spleens and tumors, respectively (Fig. 2-9 and 2-10). Systemic reduction of T cells, as well as a gradual increase in regulatory T cells (T_{reg}) in tumor-bearing hosts, have been well established [66-68]. In addition, immune contextures of growing tumors, especially tumor-infiltrating CTLs, have been shown to correlate with clinical outcomes [63]. In spleens of tumor-bearing mice, I observed drastic reduction of CD4 and CD8 T cells, generally less than 1 and 2 % among whole splenocytes, respectively (Fig. 2-9 and Fig. 2-10). In normal mice, CD4 and CD8 T cells generally occupy 20 and 10% among splenocytes, respectively [66], indicating that all the tumor-bearing mice suffered from systemic T cell suppression regardless of immunization. Nevertheless, mice immunized with PLLA fiber-ZnO nanowire composites complexed with ZBP-CEA retained significantly higher frequencies of CD4 T cells with lower T_{reg} cell proportions in spleens than other control groups. Additionally, this mice group

showed significantly higher levels of tumor-infiltrating CD4 and CD8 T cells, despite of the similar degree of CD45+ immune cells and T_{reg} cells in tumor tissues (Fig 2-10 A-B), suggesting better immune contexture in the tumor microenvironment than other control groups. These results suggest that inclusion of ZnO nanowires complexed with a tumor antigen in the therapeutic cancer vaccine formulation based on PLLA fiber matrix can enhance antigen-specific T cell responses and promotes their infiltration into tumors, thereby suppressing the tumor growth better than the complexes without ZnO nanowires.

Biocompatible PLLA-based formula has shown immense potential as a drug delivery carrier and as scaffolds for various biomedical applications [70-71]. This organic material has been successfully applied to vaccine development for infectious diseases and cancers [28, 72-76]. However, recent studies also reported that a similar organic material, polylactic-co-glycolic acid (PLGA) particles, can also induce immune tolerance against the associated peptides for treatment of autoimmune diseases, depending on particle size, shape, composition, and route of administration [77-78]. It was shown that tolerogenic effects require PLGA microparticle uptake by macrophages expressing the scavenger receptor MARCO and are mediated in part by the activity of regulatory T cells, abortive T-cell activation and T-cell anergy [78]. In addition, inert PLLA itself may have an immune suppressive effect and/or promote tissue repair and foreign body reaction, enabling them to be used as scaffolds for tissue engineering [79-80]. Therefore, considerable modification of the composition and structure of the inert organic material might be critical for biomedical applications as a vaccine carrier and/or

adjuvant [76]. Incorporation of immune-stimulating agents, such as Toll-like receptor (TLR) ligands, into the formulation is one of promising ways for cancer vaccine development to boost adaptive immunity [76]. Here, we synthesized radially grown ZnO nanowires on PLLA microfibers with unique 3-dimensional structure and applied for a therapeutic cancer vaccine. Similar hybrid composites, comprised of ZnO nanostructures and PLLA matrix, has been used for photocatalytic water purification, anti-bacterial agent, and cellular differentiation of myoblast [31-33, 81]. Nevertheless, this study is a first application of the novel hybrid nanocomposite as a vaccine adjuvant. This inorganic-organic hybrid nanocomposite has mild cellular toxicity and can efficiently stimulate innate APC, dendritic cell, to express inflammatory cytokines and activation surface markers. Induction of these innate immune responses may result from the direct recognition of ZNPs by Toll-like receptors (TLR4 or TLR6) or indirectly by intracellular ROS generation resulting from disrupted cellular zinc homeostasis [36, 59]. Induction of in vivo inflammation by ZnO nanowires was also reported previously [66]. In this study, I demonstrated that the hybrid nanocomposites could successfully induce a tumor antigen-specific cellular immunity and significantly inhibit tumor growth in vivo, potentially via efficient intracellular delivery of associated antigen into APCs as well as stimulation of innate immunity. Multifunctional interaction of ZnO nanostructures with the biological system may also enable them to be used as an attractive anticancer agent. Even though the mechanistic correlation of ZnO nanowires with systemic reduction of T_{reg} and enhanced infiltration of T cells into tumor tissues need to be further defined in the future study, These current results open a new avenue to

extend the biomedical application of inorganic metal oxide-inert organic hybrid nanocomposites [82] for cancer immune-therapeutics.

8. References

1. Zhang Y, Ram MK, Stefanakos EK, Goswami DY. Synthesis, characterization, and applications of ZnO nanowires. Journal of Nanomaterials. 2012, 22, (2012), 1-22.
2. Zhang, Y.; Nayak, T. R.; Hong, H.; Cai, W., Biomedical Applications of Zinc Oxide Nanomaterials. Current Molecular Medicine 2013, 13 (10), 1633-1645.
3. Wang, Z. L., Splendid one-dimensional nanostructures of zinc oxide: a new nanomaterial family for nanotechnology. Acs Nano 2008, 2 (10), 1987-1992.
4. Oleson, J. P., The Oxford handbook of engineering and technology in the classical world. Oxford University Press: 2010.
5. Nutting, J., 2000 years of zinc and brass. International Materials Reviews 2013, 36 (1), 81-84.
6. Craddock, P. T., The origins and inspirations of zinc smelting. Journal of materials science 2009, 44 (9), 2181-2191.
7. Lee, J.; Choi, S.; Bae, S. J.; Yoon, S. M.; Choi, J. S.; Yoon, M., Visible light-sensitive APTES-bound ZnO nanowire toward a potent nanoinjector sensing biomolecules in a living cell. Nanoscale 2013, 5 (21), 10275-10282.
8. Hong, H.; Shi, J.; Yang, Y.; Zhang, Y.; Engle, J. W.; Nickles, R. J.; Wang, X.; Cai, W., Cancer-targeted optical imaging with fluorescent zinc oxide nanowires. Nano letters 2011, 11 (9), 3744-3750.

9. Gilboa, E.; Vieweg, J., Cancer immunotherapy with mRNA- transfected dendritic cells. Immunological reviews 2004, 199 (1), 251-263.
10. Gilboa, E., DC-based cancer vaccines. Journal of Clinical Investigation 2007, 117 (5), 1195.
11. Nie, L.; Gao, L.; Feng, P.; Zhang, J.; Fu, X.; Liu, Y.; Yan, X.; Wang, T., Three-Dimensional Functionalized Tetrapod-like ZnO Nanostructures for Plasmid DNA Delivery. Small 2006, 2 (5), 621-625.
12. Prasad, A. S., Zinc in human health: effect of zinc on immune cells. Molecular medicine 2008, 14 (5-6), 353.
13. Murakami, M.; Hirano, T., Intracellular zinc homeostasis and zinc signaling. Cancer science 2008, 99 (8), 1515-1522.
14. Mandal, G.; Dass, R.; Isore, D.; Garg, A.; Ram, G., Effect of zinc supplementation from two sources on growth, nutrient utilization and immune response in male crossbred cattle (Bos indicus× Bos taurus) bulls. Animal Feed Science and Technology 2007, 138 (1), 1-12.
15. Ha, N.-Y.; Shin, H. M.; Sharma, P.; Cho, H. A.; Min, C.-K.; Kim, H.-i.; Yen, N. T. H.; Kang, J.-S.; Kim, I.-S.; Choi, M.-S., Generation of protective immunity against Orientia tsutsugamushi infection by immunization with a zinc oxide nanoparticle combined with ScaA antigen. Journal of nanobiotechnology 2016, 14 (1), 76.
16. Roy, R.; Singh, S. K.; Das, M.; Tripathi, A.; Dwivedi, P. D., Toll-like receptor 6 mediated inflammatory and functional responses of zinc oxide nanoparticles primed macrophages. Immunology 2014, 142 (3),

453-64.

17. Roy, R.; Kumar, S.; Verma, A. K.; Sharma, A.; Chaudhari, B. P.; Tripathi, A.; Das, M.; Dwivedi, P. D., Zinc oxide nanoparticles provide an adjuvant effect to ovalbumin via a Th2 response in Balb/c mice. International immunology 2013, 26 (3), 159-172.

18. Cho, N. H.; Cheong, T. C.; Min, J. H.; Wu, J. H.; Lee, S. J.; Kim, D.; Yang, J. S.; Kim, S.; Kim, Y. K.; Seong, S. Y., A multifunctional core-shell nanoparticle for dendritic cell-based cancer immunotherapy. Nat Nanotechnol 2011, 6 (10), 675-82.

19. Wang, X.; Li, X.; Ito, A.; Sogo, Y.; Watanabe, Y.; Tsuji, N. M., Hollow ZnO Nanospheres Enhance Anticancer Immunity by Promoting CD4+ and CD8+ T Cell Populations In Vivo. Small 2017, 13 (38), 1701816.

20. Rasmussen, J. W.; Martinez, E.; Louka, P.; Wingett, D. G., Zinc oxide nanoparticles for selective destruction of tumor cells and potential for drug delivery applications. Expert opinion on drug delivery 2010, 7 (9), 1063-1077.

21. Roy, R.; Parashar, V.; Chauhan, L.; Shanker, R.; Das, M.; Tripathi, A.; Dwivedi, P. D., Mechanism of uptake of ZnO nanoparticles and inflammatory responses in macrophages require PI3K mediated MAPKs signaling. Toxicology in Vitro 2014, 28 (3), 457-467.

22. Li, Z.; Yang, R.; Yu, M.; Bai, F.; Li, C.; Wang, Z. L., Cellular level biocompatibility and biosafety of ZnO nanowires. The Journal of Physical Chemistry C 2008, 112 (51), 20114-20117.

23. Pandurangan, M.; Kim, D. H., In vitro toxicity of zinc oxide

nanoparticles: a review. Journal of Nanoparticle Research 2015, 17 (3), 158.

24. Jeng, H. A.; Swanson, J., Toxicity of metal oxide nanoparticles in mammalian cells. Journal of Environmental Science and Health Part A 2006, 41 (12), 2699-2711.

25. Dalby, M. J.; Gadegaard, N.; Riehle, M. O.; Wilkinson, C. D.; Curtis, A. S., Investigating filopodia sensing using arrays of defined nano-pits down to 35 nm diameter in size. The international journal of biochemistry & cell biology 2004, 36 (10), 2005-2015.

26. Bonde, S.; Berthing, T.; Madsen, M. H.; Andersen, T. K.; Buch-Månson, N.; Guo, L.; Li, X.; Badique, F.; Anselme, K.; Nygård, J., Tuning InAs nanowire density for HEK293 cell viability, adhesion, and morphology: Perspectives for nanowire-based biosensors. ACS applied materials & interfaces 2013, 5 (21), 10510-10519.

27. Howarth M, Chinnapen DJ, Gerrow K, Dorrestein PC, Grandy MR, Kelleher NL, El-Husseini A, Ting AY. A monovalent streptavidin with a single femtomolar biotin binding site. Nature methods. 2006, 3 (4), 267.

28. Guimarães, P. P.; Oliveira, M. F.; Gomes, A. D.; Gontijo, S. M.; Cortés, M. E.; Campos, P. P.; Viana, C. T.; Andrade, S. P.; Sinisterra, R. D., PLGA nanofibers improves the antitumoral effect of daunorubicin. Colloids and Surfaces B: Biointerfaces 2015, 136, 248-255.

29. Bae, M. Y.; Cho, N. H.; Seong, S. Y., Protective anti-tumour immune responses by murine dendritic cells pulsed with recombinant Tat-

carcinoembryonic antigen derived from Escherichia coli. Clinical and experimental immunology 2009, 157 (1), 128-38.

30. Cheong, T.-C.; Shin, E. P.; Kwon, E.-K.; Choi, J.-H.; Wang, K.-K.; Sharma, P.; Choi, K. H.; Lim, J.-M.; Kim, H.-G.; Oh, K., Functional manipulation of dendritic cells by photoswitchable generation of intracellular reactive oxygen species. ACS chemical biology 2014, 10 (3), 757-765.

31. Burks, T.; Akthar, F.; Saleemi, M.; Avila, M.; Kiros, Y., ZnO-PLLA Nanofiber Nanocomposite for Continuous Flow Mode Purification of Water from Cr(VI). Journal of Environmental and Public Health 2015, 2015, 7.

32. Abhilash, S.; K., G. V.; Abdusalam, U.; S., T. M.; Mamoun, M., Radially Oriented ZnO Nanowires on Flexible Poly- l- Lactide Nanofibers for Continuous- Flow Photocatalytic Water Purification. Journal of the American Ceramic Society 2010, 93 (11), 3740-3744.

33. Trujillo, S.; Lizundia, E.; Vilas, J. L.; Salmeron-Sanchez, M., PLLA/ZnO nanocomposites: Dynamic surfaces to harness cell differentiation. Colloids and Surfaces B: Biointerfaces 2016, 144, 152-160.

34. Zhang, Z. Y.; Xu, Y. D.; Ma, Y. Y.; Qiu, L. L.; Wang, Y.; Kong, J. L.; Xiong, H. M., Biodegradable ZnO@polymer core-shell nanocarriers: pH-triggered release of doxorubicin in vitro. Angewandte Chemie 2013, 52 (15), 4127-31.

35. Bae, S.; Park, S.; Kim, J.; Choi, J. S.; Kim, K. H.; Kwon, D.; Jin, E.; Park, I.; Kim, D. H.; Seo, T. S., Exogenous Gene Integration for

Microalgal Cell Transformation Using a Nanowire-Incorporated Microdevice. Acs Applied Materials & Interfaces 2015, 7 (49), 27554-27561.

36. Saptarshi, S. R.; Duschl, A.; Lopata, A. L., Biological reactivity of zinc oxide nanoparticles with mammalian test systems: an overview. Nanomedicine 2015, 10 (13), 2075-92.

37. Sruthi, S.; Mohanan, P. V., Engineered zinc oxide nanoparticles; biological interactions at the organ level. Current medicinal chemistry 2016.

38. James, S. A.; Feltis, B. N.; de Jonge, M. D.; Sridhar, M.; Kimpton, J. A.; Altissimo, M.; Mayo, S.; Zheng, C.; Hastings, A.; Howard, D. L.; Paterson, D. J.; Wright, P. F.; Moorhead, G. F.; Turney, T. W.; Fu, J., Quantification of ZnO nanoparticle uptake, distribution, and dissolution within individual human macrophages. ACS Nano 2013, 7 (12), 10621-35.

39. Papavlassopoulos, H.; Mishra, Y. K.; Kaps, S.; Paulowicz, I.; Abdelaziz, R.; Elbahri, M.; Maser, E.; Adelung, R.; Rohl, C., Toxicity of functional nano-micro zinc oxide tetrapods: impact of cell culture conditions, cellular age and material properties. PLoS One 2014, 9 (1), e84983.

40. Nie, L.; Gao, L.; Feng, P.; Zhang, J.; Fu, X.; Liu, Y.; Yan, X.; Wang, T., Three- Dimensional Functionalized Tetrapod- like ZnO Nanostructures for Plasmid DNA Delivery. Small 2006, 2 (5), 621-625.

41. Cho, J. W.; Lee, C. S.; Lee, K. I.; Kim, S. M.; Kim, S. H.; Kim, Y. K.,

Morphology and electrical properties of high aspect ratio ZnO nanowires grown by hydrothermal method without repeated batch process. Applied Physics Letters 2012, 101 (8).

42. Deng, J.; Wang, M.; Song, X.; Liu, J., Controlled synthesis of aligned ZnO nanowires and the application in CdSe-sensitized solar cells. Journal of Alloys and Compounds 2014, 588, 399-405.

43. Xu, S.; Lao, C.; Weintraub, B.; Wang, Z. L., Density-controlled growth of aligned ZnO nanowire arrays by seedless chemical approach on smooth surfaces. Journal of Materials Research 2008, 23 (08), 2072-2077.

44. Woo Cho, J.; Seung Lee, C.; Il Lee, K.; Min Kim, S.; Hyun Kim, S.; Keun Kim, Y., Morphology and electrical properties of high aspect ratio ZnO nanowires grown by hydrothermal method without repeated batch process. Applied Physics Letters 2012, 101 (8), 083905.

45. Wan, Q.; Li, Q. H.; Chen, Y. J.; Wang, T. H.; He, X. L.; Li, J. P.; Lin, C. L., Fabrication and ethanol sensing characteristics of ZnO nanowire gas sensors. Applied Physics Letters 2004, 84 (18), 3654-3656.

46. Garner, M. M.; Revzin, A., A gel electrophoresis method for quantifying the binding of proteins to specific DNA regions: application to components of the Escherichia coli lactose operon regulatory system. Nucleic acids research 1981, 9 (13), 3047-3060.

47. Liang, M.-K.; Deschaume, O.; Patwardhan, S. V.; Perry, C. C., Direct evidence of ZnO morphology modification via the selective adsorption of ZnO-binding peptides. Journal of Materials Chemistry

2011, 21 (1), 80-89.

48. Shalek, A. K.; Robinson, J. T.; Karp, E. S.; Lee, J. S.; Ahn, D. R.; Yoon, M. H.; Sutton, A.; Jorgolli, M.; Gertner, R. S.; Gujral, T. S.; MacBeath, G.; Yang, E. G.; Park, H., Vertical silicon nanowires as a universal platform for delivering biomolecules into living cells. Proc Natl Acad Sci U S A 2010, 107 (5), 1870-5.

49. Niepelt, R.; Schröder, U. C.; Sommerfeld, J.; Slowik, I.; Rudolph, B.; Möller, R.; Seise, B.; Csaki, A.; Fritzsche, W.; Ronning, C., Biofunctionalization of zinc oxide nanowires for DNA sensory applications. Nanoscale research letters 2011, 6 (1), 1.

50. Xie, X.; Xu, A. M.; Angle, M. R.; Tayebi, N.; Verma, P.; Melosh, N. A., Mechanical model of vertical nanowire cell penetration. Nano Lett 2013, 13 (12), 6002-8.

51. Shi, X.; von dem Bussche, A.; Hurt, R. H.; Kane, A. B.; Gao, H., Cell entry of one-dimensional nanomaterials occurs by tip recognition and rotation. Nat Nanotechnol 2011, 6 (11), 714-9.

52. Yi, X.; Shi, X.; Gao, H., A universal law for cell uptake of one-dimensional nanomaterials. Nano Lett 2014, 14 (2), 1049-55.

53. Aalipour, A.; Xu, A. M.; Leal-Ortiz, S.; Garner, C. C.; Melosh, N. A., Plasma Membrane and Actin Cytoskeleton as Synergistic Barriers to Nanowire Cell Penetration. Langmuir 2014, 30 (41), 12362-12367.

54. Kwak, M.; Han, L.; Chen, J. J.; Fan, R., Interfacing Inorganic Nanowire Arrays and Living Cells for Cellular Function Analysis. Small 2015, 11 (42), 5600-10.

55. Xie, X.; Aalipour, A.; Gupta, S. V.; Melosh, N. A., Determining the

Time Window for Dynamic Nanowire Cell Penetration Processes. ACS Nano 2015, 9 (12), 11667-77.

56. Xu, A. M.; Aalipour, A.; Leal-Ortiz, S.; Mekhdjian, A. H.; Xie, X.; Dunn, A. R.; Garner, C. C.; Melosh, N. A., Quantification of nanowire penetration into living cells. Nat Commun 2014, 5.

57. Xiong, H. M., ZnO nanoparticles applied to bioimaging and drug delivery. Adv Mater 2013, 25 (37), 5329-35.

58. Roy, R.; Kumar, S.; Verma, A. K.; Sharma, A.; Chaudhari, B. P.; Tripathi, A.; Das, M.; Dwivedi, P. D., Zinc oxide nanoparticles provide an adjuvant effect to ovalbumin via a Th2 response in Balb/c mice. Int Immunol 2014, 26 (3), 159-72.

59. Roy, R.; Das, M.; Dwivedi, P. D., Toxicological mode of action of ZnO nanoparticles: Impact on immune cells. Mol Immunol 2015, 63 (2), 184-92.

60. Saptarshi, S. R.; Feltis, B. N.; Wright, P. F. A.; Lopata, A. L., Investigating the immunomodulatory nature of zinc oxide nanoparticles at sub-cytotoxic levels in vitro and after intranasal instillation in vivo. Journal of Nanobiotechnology 2015, 13.

61. Palomaki, J.; Karisola, P.; Pylkkanen, L.; Savolainen, K.; Alenius, H., Engineered nanomaterials cause cytotoxicity and activation on mouse antigen presenting cells. Toxicology 2010, 267 (1-3), 125-31.

62. Blum, J. S.; Wearsch, P. A.; Cresswell, P., Pathways of antigen processing. Annu Rev Immunol 2013, 31, 443-73.

63. Yang, H.; Cho, N. H.; Seong, S. Y., The Tat-conjugated N-terminal region of mucin antigen 1 (MUC1) induces protective immunity

against MUC1-expressing tumours. Clinical and experimental immunology 2009, 158 (2), 174-85.

64. Fridman, W. H.; Pages, F.; Sautes-Fridman, C.; Galon, J., The immune contexture in human tumours: impact on clinical outcome. Nat Rev Cancer 2012, 12 (4), 298-306.

65. Mildner, A.; Jung, S., Development and function of dendritic cell subsets. Immunity 2014, 40 (5), 642-56.

66. Zaveri, T. D.; Dolgova, N. V.; Chu, B. H.; Lee, J.; Wong, J.; Lele, T. P.; Ren, F.; Keselowsky, B. G., Contributions of surface topography and cytotoxicity to the macrophage response to zinc oxide nanorods. Biomaterials 2010, 31 (11), 2999-3007.

67. Radoja, S.; Rao, T. D.; Hillman, D.; Frey, A. B., Mice bearing late-stage tumors have normal functional systemic T cell responses in vitro and in vivo. J Immunol 2000, 164 (5), 2619-2628.

68. Liu, J. Y.; Zhang, X. S.; Ding, Y.; Peng, R. Q.; Cheng, X.; Zhang, N. H.; Xia, J. C.; Zeng, Y. X., The changes of CD4+CD25+/CD4+ proportion in spleen of tumor-bearing BALB/c mice. J Transl Med 2005, 3 (1), 5.

69. Oleinika, K.; Nibbs, R. J.; Graham, G. J.; Fraser, A. R., Suppression, subversion and escape: the role of regulatory T cells in cancer progression. Clinical and experimental immunology 2013, 171 (1), 36-45.

70. Chen, A.; Dang, T.; Wang, S.; Tang, N.; Liu, Y.; Wu, W., The in vitro and in vivo anti-tumor effects of MTX-Fe3O4-PLLA-PEG-PLLA microspheres prepared by suspension-enhanced dispersion by

supercritical CO2. Science China Life Sciences 2014, 57 (7), 698-709.

71. Saini, P.; Arora, M.; Kumar, M., Poly(lactic acid) blends in biomedical applications. Adv Drug Deliv Rev 2016, 107, 47-59.

72. Eyles, J. E.; Bramwell, V. W.; Williamson, E. D.; Alpar, H. O., Microsphere translocation and immunopotentiation in systemic tissues following intranasal administration. Vaccine 2001, 19 (32), 4732-42.

73. Coumes, F.; Huang, C. Y.; Huang, C. H.; Coudane, J.; Domurado, D.; Li, S.; Darcos, V.; Huang, M. H., Design and Development of Immunomodulatory Antigen Delivery Systems Based on Peptide/PEG-PLA Conjugate for Tuning Immunity. Biomacromolecules 2015, 16 (11), 3666-73.

74. Wang, J.; Li, S.; Han, Y.; Guan, J.; Chung, S.; Wang, C.; Li, D., Poly(Ethylene Glycol)-Polylactide Micelles for Cancer Therapy. Front Pharmacol 2018, 9, 202.

75. Di Bonito, P.; Petrone, L.; Casini, G.; Francolini, I.; Ammendolia, M. G.; Accardi, L.; Piozzi, A.; D'Ilario, L.; Martinelli, A., Amino-functionalized poly(L-lactide) lamellar single crystals as a valuable substrate for delivery of HPV16-E7 tumor antigen in vaccine development. International Journal of Nanomedicine 2015, 10, 3447-3458.

76. Silva, J. M.; Videira, M.; Gaspar, R.; Preat, V.; Florindo, H. F., Immune system targeting by biodegradable nanoparticles for cancer vaccines. J Control Release 2013, 168 (2), 179-99.

77. Hunter, Z.; McCarthy, D. P.; Yap, W. T.; Harp, C. T.; Getts, D. R.; Shea, L. D.; Miller, S. D., A biodegradable nanoparticle platform for the induction of antigen-specific immune tolerance for treatment of autoimmune disease. ACS Nano 2014, 8 (3), 2148-60.

78. Getts, D. R.; Martin, A. J.; McCarthy, D. P.; Terry, R. L.; Hunter, Z. N.; Yap, W. T.; Getts, M. T.; Pleiss, M.; Luo, X.; King, N. J.; Shea, L. D.; Miller, S. D., Microparticles bearing encephalitogenic peptides induce T-cell tolerance and ameliorate experimental autoimmune encephalomyelitis. Nat Biotechnol 2012, 30 (12), 1217-24.

79. Kadowaki, S.; Sugimoto, K.; Tsurumaki, Y.; Tabata, Y.; Ikada, Y.; Fujita, J.; Mori, K. J., Application of poly(L-lactic acid) particles for the suppression of genetic resistance to bone marrow allografts by reticuloendothelial system-blockade. Biomed Pharmacother 1993, 47 (9), 385-91.

80. Santoro, M.; Shah, S. R.; Walker, J. L.; Mikos, A. G., Poly(lactic acid) nanofibrous scaffolds for tissue engineering. Adv Drug Deliv Rev 2016, 107, 206-212.

81. Rodriguez-Tobias, H.; Morales, G.; Ledezma, A.; Romero, J.; Grande, D., Novel antibacterial electrospun mats based on poly(d,l-lactide) nanofibers and zinc oxide nanoparticles. Journal of Materials Science 2014, 49 (24), 8373-8385.

82. Mir SH, Nagahara LA, Thundat T, Mokarian-Tabari P, Furukawa H, Khosla A. Organic-inorganic hybrid functional materials: An integrated platform for applied technologies. Journal of The Electrochemical Society. 2018, 1;165(8), B3137-56.

83. Greene, L. E.; Law, M.; Goldberger, J.; Kim, F.; Johnson, J. C.; Zhang, Y. F.; Saykally, R. J.; Yang, P. D., Low-temperature wafer-scale production of ZnO nanowire arrays. Angew Chem Int Edit 2003, 42 (26), 3031-3034.

84. Pacholski, C.; Kornowski, A.; Weller, H., Self-assembly of ZnO: from nanodots to nanorods. Angewandte Chemie 2002, 41 (7), 1188-91.

85. Palacio, J.; Orozco, V. H.; Lopez, B. L., Effect of the Molecular Weight on the Physicochemical Properties of Poly(lactic acid) Nanoparticles and on the Amount of Ovalbumin Adsorption. J Brazil Chem Soc 2011, 22 (12), 2304-2311.

86. Pachynski RK, Scholz A, Monnier J, Butcher EC, Zabel BA. Evaluation of tumor-infiltrating leukocyte subsets in a subcutaneous tumor model. JoVE (Journal of Visualized Experiments). 2015, 4 (98):e52657.

국문 초록

산화아연(zinc oxide, ZnO) 나노복합체는 다양한 기능과 생체적합성 때문에 의공학 분야에서 광범위하게 사용되고 있다. 그러나 산화아연 나노복합체와 생물학적 시스템 또는 면역체계와의 상호작용 및 그 물리, 화학적 특성은 아직 잘 밝혀지지 않았다. 산화아연 나노선의 의학적 활용가능성을 알아보기 위하여, 본 연구에서는 산화아연 나노선을 커버슬립 위에 수직 형태(vertical nanowire, VNW) 혹은 부채꼴 형태(fan-shaped nanowire, FNW)로 코팅한 후, 그 위에 세포를 배양하여 각각의 세포 활성도의 변화를 측정하였다. VNW 와 FNW 산화아연 나노선에서 배양한 HEK293 세포는 배양 후 6시간까지 세포사멸이 증가하였지만, 그 후 12시간까지는 유의할 만한 세포사멸을 보이지 않으며 생존하였다. FNW에서 자란 세포는 표면을 감싸는 층상위족(lamellipodia)을 형성하였고, 나노선에 결합된 ZBP-FITC를 30분내에 효과적으로 세포내로 섭취하였다. 또한, FNW에 결합한 DNA를 세포 내로 전달하고 세포에서 단백질로 발현되는 것을 확인함으로써, FNW에 의해 외부의 DNA를 핵 내부로 전달할 수 있음을 증명하였다. 이 결과로, 산화아연 나노선 배열이 적절한 3차원 구조를 가진다면 효과적인 나노-바이오 결합체로써 작용할 수 있음을 알 수 있었다. 그에 따라, 폴리젖산 미세섬유에 산화아연 나노선을 방사형으로 자라나게 한 독특한 3차원 구조물을 합성하였고, 치료용

암 백신으로써 산화아연 나노복합체의 항-종양 면역능을 검증하였다. 이 무기물-유기물 하이브리드 나노복합체는 낮은 세포독성을 띠며, 결합된 종양 항원을 효과적으로 수지상세포 안으로 전달하고 세포가 염증성 사이토카인을 발현하게 하여, 선천면역과 적응면역을 연결하는 역할을 하는 것으로 관찰되었다. 이 복합체는 항원-특이적 세포 면역을 효과적으로 유도하며, 종양의 성장을 유의하게 억제하였다. 생체 전반적인 조절 T 세포가 감소하고 종양 조직으로 T 세포의 유입이 증가하였다. 무기물-유기물 하이브리드 나노복합체를 활용하여 항암면역치료에 적용함으로써 새로운 백신 플랫폼으로의 가능성을 보였다.

주요어 : 산화아연 나노선, 세포내 전달, 폴리젖산 중합체 미세섬유, 산화아연-결합 펩티드, 무기물-유기물 하이브리드, 항암면역치료

Student number: 2013-30817